Diwan A, Krenz M, Syed FM *et al.* (2007) Inhibition of ischemic cardiomyocyte apoptosis through targeted ablation of Bnip3 restrains postinfarction remodeling in mice. *J Clin Invest* 117:2825–33

Feng X, Liu X, Zhang W *et al.* (2011) p53 directly suppresses BNIP3 expression to protect against hypoxia-induced cell death. *EMBO J* 30: 3397–415

Gilchrest BA, Soter NA, Stoff JS *et al.* (1981) The human sunburn reaction: histologic and biochemical studies. *J Am Acad Dermatol* 5:411–22

Hamacher-Brady A, Brady NR, Logue SE *et al.* (2007) Response to myocardial ischemia/reperfusion injury involves Bnip3 and autophagy. *Cell Death Differ* 14:146–57

Haruna K, Suga Y, Muramatsu S *et al.* (2008) Differentiation-specific expression and localization of an autophagosomal marker protein (LC3) in human epidermal keratinocytes. *J Dermatol Sci* 52:213–5

Ishibashi M, Moriyoshi K, Sasai Y *et al.* (1994) Persistent expression of helix-loop-helix factor HES-1 prevents mammalian neural differentiation in the central nervous system. *EMBO J* 13:1799–805

Itoh T, Itoh A, Pleasure D (2003) Bcl-2-related protein family gene expression during oligodendroglial differentiation. *J Neurochem* 85:1500–12

Juenemann K, Reits EA (2012) Alternative macroautophagic pathways. *Int J Cell Biol* 2012:189794

Kabeya Y, Mizushima N, Ueno T *et al.* (2000) LC3, a mammalian homologue of yeast Apg8p, is localized in autophagosome membranes after processing. *EMBO J* 19:5720–8

Knowles HJ, Athanasou NA (2008) Hypoxia-inducible factor is expressed in giant cell tumour of bone and mediates paracrine effects of hypoxia on monocyte-osteoclast differentiation via induction of VEGF. *J Pathol* 215:56–66

Lippens S, Denecker G, Ovaere P *et al.* (2005) Death penalty for keratinocytes: apoptosis versus cornification. *Cell Death Differ* 12(Suppl 2):1497–508

Mellor HR, Rouschop KM, Wigfield SM *et al.* (2010) Synchronised phosphorylation of BNIP3, Bcl-2 and Bcl-xL in response to microtubule-active drugs is JNK-independent and requires a mitotic kinase. *Biochem Pharmacol* 79:1562–72

Mizushima N, Levine B (2010) Autophagy in mammalian development and differentiation. *Nat Cell Biol* 12:823–30

Mizushima N, Yamamoto A, Matsui M *et al.* (2004) In vivo analysis of autophagy in response to nutrient starvation using transgenic mice expressing a fluorescent autophagosome marker. *Mol Biol Cell* 15:1101–11

Mizushima N, Yoshimori T, Levine B (2010) Methods in mammalian autophagy research. *Cell* 140:313–26

Moriyama H, Moriyama M, Sawaragi K *et al.* (2013) Tightly regulated and homogeneous transgene expression in human adipose-derived mesenchymal stem cells by lentivirus with tet-off system. *PLoS One* 8:e66274

Moriyama M, Durham AD, Moriyama H *et al.* (2008) Multiple roles of Notch signaling in the regulation of epidermal development. *Dev Cell* 14:594–604

Moriyama M, Moriyama H, Ueda A *et al.* (2012) Human adipose tissue-derived multilineage progenitor cells exposed to oxidative stress induce neurite outgrowth in PC12 cells through p38 MAPK signaling. *BMC Cell Biol* 13:21

Moriyama M, Osawa M, Mak SS *et al.* (2006) Notch signaling via Hes1 transcription factor maintains survival of melanoblasts and melanocyte stem cells. *J Cell Biol* 173:333–9

Nishida Y, Arakawa S, Fujitani K *et al.* (2009) Discovery of Atg5/Atg7-independent alternative macroautophagy. *Nature* 461:654–8

Ohtsuka T, Ishibashi M, Gradwohl G *et al.* (1999) Hes1 and Hes5 as notch effectors in mammalian neuronal differentiation. *EMBO J* 18:2196–207

Quinsay MN, Thomas RL, Lee Y *et al.* (2010) Bnip3-mediated mitochondrial autophagy is independent of the mitochondrial permeability transition pore. *Autophagy* 6:855–62

Rossiter H, Konig U, Barresi C *et al.* (2013) Epidermal keratinocytes form a functional skin barrier in the absence of Atg7 dependent autophagy. *J Dermatol Science* 71:67–75

Sassone J, Colciago C, Marchi P *et al.* (2010) Mutant Huntingtin induces activation of the Bcl-2/adenovirus E1B 19-kDa interacting protein (BNip3). *Cell Death Dis* 1:e7

Schweers RL, Zhang J, Randall MS *et al.* (2007) NIX is required for programmed mitochondrial clearance during reticulocyte maturation. *Proc Natl Acad Sci USA* 104:19500–5

Sowter HM, Ratcliffe PJ, Watson P *et al.* (2001) HIF-1-dependent regulation of hypoxic induction of the cell death factors BNIP3 and NIX in human tumors. *Cancer Res* 61:6669–73

Srinivas V, Bohensky J, Shapiro IM (2009) Autophagy: a new phase in the maturation of growth plate chondrocytes is regulated by HIF, mTOR and AMP kinase. *Cells Tissues Organs* 189:88–92

Tron VA, Trotter MJ, Tang L *et al.* (1998) p53-regulated apoptosis is differentiation dependent in ultraviolet B-irradiated mouse keratinocytes. *Am J Pathol* 153:579–85

Vengellur A, LaPres JJ (2004) The role of hypoxia inducible factor 1alpha in cobalt chloride induced cell death in mouse embryonic fibroblasts. *Toxicol Sci* 82:638–46

Walls KC, Ghosh AP, Ballestas ME *et al.* (2009) bcl-2/Adenovirus E1B 19-kd interacting protein 3 (BNIP3) regulates hypoxia-induced neural precursor cell death. *J Neuropathol Exp Neurol* 68:1326–38

Young AR (1987) The sunburn cell. *Photodermatology* 4:127–34

Zhang J, Ney PA (2009) Role of BNIP3 and NIX in cell death, autophagy, and mitophagy. *Cell Death Differ* 16:939–46

Zhao Y, Chen G, Zhang W *et al.* (2012) Autophagy regulates hypoxia-induced osteoclastogenesis through the HIF-1alpha/BNIP3 signaling pathway. *J Cell Physiol* 227:639–48

Zhao Y, Zhang CF, Rossiter H *et al.* (2013) Autophagy is induced by UVA and promotes removal of oxidized phospholipids and protein aggregates in epidermal keratinocytes. *J Invest Dermatol* 133:1629–37

© 2014. Published by The Company of Biologists Ltd | Development (2014) 141, 91-100 doi:10.1242/dev.103168

RESEARCH ARTICLE

STEM CELLS AND REGENERATION

CCAAT/enhancer binding protein-mediated regulation of TGFβ receptor 2 expression determines the hepatoblast fate decision

Kazuo Takayama[1,2,3], Kenji Kawabata[4], Yasuhito Nagamoto[1,2], Mitsuru Inamura[1], Kazuo Ohashi[5], Hiroko Okuno[1], Tomoko Yamaguchi[4], Katsuhisa Tashiro[4], Fuminori Sakurai[1], Takao Hayakawa[6], Teruo Okano[5], Miho Kusada Furue[7,8] and Hiroyuki Mizuguchi[1,2,3,9,*]

ABSTRACT

Human embryonic stem cells (hESCs) and their derivatives are expected to be used in drug discovery, regenerative medicine and the study of human embryogenesis. Because hepatocyte differentiation from hESCs has the potential to recapitulate human liver development *in vivo*, we employed this differentiation method to investigate the molecular mechanisms underlying human hepatocyte differentiation. A previous study has shown that a gradient of transforming growth factor beta (TGFβ) signaling is required to segregate hepatocyte and cholangiocyte lineages from hepatoblasts. Although CCAAT/enhancer binding proteins (c/EBPs) are known to be important transcription factors in liver development, the relationship between TGFβ signaling and c/EBP-mediated transcriptional regulation in the hepatoblast fate decision is not well known. To clarify this relationship, we examined whether c/EBPs could determine the hepatoblast fate decision via regulation of TGFβ receptor 2 (TGFBR2) expression in the hepatoblast-like cells differentiated from hESCs. We found that *TGFBR2* promoter activity was negatively regulated by c/EBPα and positively regulated by c/EBPβ. Moreover, c/EBPα overexpression could promote hepatocyte differentiation by suppressing TGFBR2 expression, whereas c/EBPβ overexpression could promote cholangiocyte differentiation by enhancing TGFBR2 expression. Our findings demonstrated that c/EBPα and c/EBPβ determine the lineage commitment of hepatoblasts by negatively and positively regulating the expression of a common target gene, *TGFBR2*, respectively.

KEY WORDS: Hepatoblasts, c/EBP, CEBP, Human ESCs

INTRODUCTION

Many animal models, such as chick, *Xenopus*, zebrafish and mouse, have been used to investigate the molecular mechanisms of liver development. Because many functions of the key molecules in liver development are conserved in these species, studies on liver development in these animals can be highly informative with respect that in humans. However, some functions of important molecules in liver development might differ between human and other species. Although analysis using genetically modified mice has been successfully performed, it is not of course possible to perform genetic experiments to elucidate molecular mechanisms of liver development in human. Pluripotent stem cells, such as human embryonic stem cells (hESCs), are expected to overcome some of these problems in the study of human embryogenesis, including liver development, because the gene expression profiles of this model are similar to those in normal liver development (Agarwal et al., 2008; DeLaForest et al., 2011).

During liver development, hepatoblasts differentiate into hepatocytes and cholangiocytes. A previous study has shown that a high concentration of transforming growth factor beta (TGFβ) could give rise to cholangiocyte differentiation from hepatoblasts (Clotman et al., 2005). To transmit the TGFβ signaling, TGFβ receptor 2 (TGFBR2) has to be stimulated by TGFβ1, TGFβ2 or TGFβ3 (Kitisin et al., 2007). TGFβ binding to the extracellular domain of TGFBR2 induces a conformational change, resulting in the phosphorylation and activation of TGFBR1. TGFBR1 phosphorylates SMAD2 or SMAD3, which binds to SMAD4, and then the SMAD complexes move into the nucleus and function as transcription factors to express various kinds of differentiation-related genes (Kitisin et al., 2007). Although the function of TGFBR2 in regeneration of the adult liver has been thoroughly examined (Oe et al., 2004), the function of TGFBR2 in the hepatoblast fate decision has not been elucidated.

CCAAT/enhancer binding protein (c/EBP) transcription factors play decisive roles in the differentiation of various cell types, including hepatocytes (Tomizawa et al., 1998; Yamasaki et al., 2006). The analysis of *c/EBPα* (*Cebpa*) knockout mice has shown that many abnormal pseudoglandular structures, which co-express antigens specific for both hepatocytes and cholangiocytes, are present in the liver parenchyma (Tomizawa et al., 1998). These data demonstrated that c/EBPα plays an important role in hepatocyte differentiation. It is also known that the suppression of c/EBPα expression in periportal hepatoblasts stimulates cholangiocyte differentiation (Yamasaki et al., 2006). Although the function of c/EBPα in liver development is well known, the relationship between TGFβ signaling and c/EBPα-mediated transcriptional regulation in the hepatoblast fate decision is poorly understood. c/EBPβ is also known to be an important factor for liver function (Chen et al., 2000), although the function of c/EBPβ in the cell fate decision of hepatoblasts is not well known. c/EBPα and c/EBPβ bind to the same DNA binding site. However, the promoter activity of hepatocyte-specific genes, such as those encoding hepatocyte nuclear factor 6 (HNF6, also known as ONECUT1) and UGT2B1,

[1]Laboratory of Biochemistry and Molecular Biology, Graduate School of Pharmaceutical Sciences, Osaka University, Osaka 565-0871, Japan. [2]Laboratory of Hepatocyte Differentiation, National Institute of Biomedical Innovation, Osaka 567-0085, Japan. [3]iPS Cell-based Research Project on Hepatic Toxicity and Metabolism, Graduate School of Pharmaceutical Sciences, Osaka University, Osaka 565-0871, Japan. [4]Laboratory of Stem Cell Regulation, National Institute of Biomedical Innovation, Osaka 567-0085, Japan. [5]Institute of Advanced Biomedical Engineering and Science, Tokyo Women's Medical University, Tokyo 162-8666, Japan. [6]Pharmaceutical Research and Technology Institute, Kinki University, Osaka 577-8502, Japan. [7]Laboratory of Embryonic Stem Cell Cultures, Department of Disease Bioresources Research, National Institute of Biomedical Innovation, Osaka 567-0085, Japan. [8]Department of Embryonic Stem Cell Research, Field of Stem Cell Research, Institute for Frontier Medical Sciences, Kyoto University, Kyoto 606-8507, Japan. [9]The Center for Advanced Medical Engineering and Informatics, Osaka University, Osaka 565-0871, Japan.

*Author for correspondence (mizuguch@phs.osaka-u.ac.jp)

Received 27 August 2013; Accepted 3 October 2013

is positively regulated by c/EBPα but not c/EBPβ (Hansen et al., 1998; Plumb-Rudewiez et al., 2004), suggesting that the functions of c/EBPα and c/EBPβ in the hepatoblast fate decision might be different.

In the present study, we first examined the function of TGFBR2 in the hepatoblast fate decision using hESC-derived hepatoblast-like cells, which have the ability to self-replicate, differentiate into both hepatocyte and cholangiocyte lineages, and repopulate the liver of carbon tetrachloride (CCl_4)-treated immunodeficient mice. *In vitro* gain- and loss-of-function analyses and *in vivo* transplantation analysis were performed. Next, we investigated how TGFBR2 expression is regulated in the hepatoblast fate decision. Finally, we examined whether our findings could be reproduced in delta-like 1 homolog (Dlk1)-positive hepatoblasts obtained from the liver of E13.5 mice. To the best of our knowledge, this study provides the first evidence of c/EBP-mediated regulation of TGFBR2 expression in the human hepatoblast fate decision.

RESULTS

Hepatoblast-like cells are generated from hESCs

First, we investigated whether the hepatoblast-like cells (HBCs), which were differentiated from hESCs as described in supplementary material Fig. S1A, have similar characteristics to human hepatoblasts. We recently found that hESC-derived HBCs could be purified and maintained on human laminin 111 (LN111)-coated dishes (Takayama et al., 2013). The long-term cultured HBC population (HBCs passaged more than three times were used in this study) were nearly homogeneous and expressed human hepatoblast markers such as alpha-fetoprotein (AFP), albumin (ALB), cytokeratin 19 (CK19, also known as KRT19) and EPCAM (Schmelzer et al., 2007) (supplementary material Fig. S1B). In addition, most of the colonies observed on human LN111-coated plates were ALB and CK19 double positive, although a few colonies were ALB single positive, CK19 single positive, or ALB and CK19 double negative (supplementary material Fig. S1C). To examine the hepatocyte differentiation capacity of the HBCs *in vivo*, these cells were transplanted into CCl_4-treated immunodeficient mice. The hepatocyte functionality of the transplanted cells was assessed by measuring secreted human ALB levels in the recipient mice (supplementary material Fig. S1D). Human ALB serum was detected in the mice that were transplanted with the HBCs, but not in the control mice. These results demonstrated that the HBCs generated from hESCs have similar characteristics to human hepatoblasts and would therefore provide a valuable tool to investigate the mechanisms of human liver development. In the present study, HBCs generated from hESCs were used to elucidate the mechanisms of the hepatoblast fate decision.

TGFBR2 expression is decreased in hepatocyte differentiation but increased in cholangiocyte differentiation

The HBCs used in this study have the ability to differentiate into both hepatocyte-like cells [cytochrome P450 3A4 (CYP3A4) positive; Fig. 1B] and cholangiocyte-like cells (CK19 positive; Fig. 1C) (the protocols are described in Fig. 1A). Because the expression pattern of TGFBR2 during differentiation from hepatoblasts is not well known, we examined it in hepatocyte and cholangiocyte differentiation from HBCs. *TGFBR2* was downregulated during hepatocyte differentiation from HBCs (Fig. 1D), but upregulated in cholangiocyte differentiation from HBCs (Fig. 1E). After the HBCs were cultured on Matrigel, the cells were fractionated into three populations according to the level of TGFBR2 expression (TGFBR2-negative, -lo or -hi; Fig. 1F). The HBC-derived TGFBR2-lo cells strongly expressed *αAT* and *CYP3A4* (hepatocyte markers), whereas the HBC-derived TGFBR2-hi cells strongly expressed *SOX9* and integrin β4 (*ITGB4*) (cholangiocyte markers). These data suggest that the TGFBR2 expression level is decreased in hepatic differentiation, but increased in biliary differentiation of the HBCs.

The cell fate decision of HBCs is regulated by TGFβ signals

To examine the function of TGFβ1, β2 and β3 (all of which are ligands of TGFBR2) in the hepatoblast fate decision, HBCs were cultured in medium containing TGFβ1, β2 or β3 (Fig. 2A,B). The expression levels of cholangiocyte marker genes were upregulated by addition of TGFβ1 or TGFβ2, but not TGFβ3 (Fig. 2A), whereas those of hepatocyte markers were downregulated by addition of TGFβ1 or TGFβ2 (Fig. 2B). To ascertain that TGFBR2 is also important in the hepatoblast fate decision, HBCs were cultured in medium containing SB-431542, which inhibits TGFβ signaling (Fig. 2C,D). Hepatocyte marker genes were upregulated by inhibition of TGFβ signaling (Fig. 2C), whereas cholangiocyte markers were downregulated (Fig. 2D). To confirm the function of TGFβ1, β2 and β3 in the hepatoblast fate decision, colony assays of the HBCs were performed in the presence or absence of TGFβ1, β2 or β3 (Fig. 2E). The number of CK19 single-positive colonies was significantly increased in TGFβ1- or β2-treated HBCs. By contrast, the number of ALB and CK19 double-positive colonies was reduced in TGFβ1-, β2- or β3-treated HBCs. These data indicated that TGFβ1 and β2 positively regulate the biliary differentiation of HBCs. Taken together, the findings suggested that TGFBR2 might be a key molecule in the regulation of hepato-bilary lineage segregation.

TGFBR2 plays an important role in the cell fate decision of HBCs

To examine whether TGFBR2 plays an important role in the hepatoblast fate decision, *in vitro* gain- and loss-of-function analysis of TGFBR2 was performed in the HBCs. We used siRNA in knockdown experiments (supplementary material Fig. S2) during HBC differentiation on Matrigel. Whereas TGFBR2-suppressing siRNA (si-TGFBR2) transfection upregulated the expression of hepatocyte markers, it downregulated cholangiocyte markers (Fig. 3A). si-TGFBR2 transfection increased the percentage of asialoglycoprotein receptor 1 (ASGR1)-positive hepatocyte-like cells (Fig. 3B). By contrast, it decreased the percentage of aquaporin 1 (AQP1)-positive cholangiocyte-like cells. These results suggest that TGFBR2 knockdown promotes hepatocyte differentiation, whereas it inhibits cholangiocyte differentiation. Next, we used Ad vector to perform efficient transduction into the HBCs (supplementary material Fig. S3) and ascertained *TGFBR2* gene expression in TGFBR2-expressing Ad vector (Ad-TGFBR2)-transduced cells (supplementary material Fig. S4). Ad-TGFBR2 transduction downregulated the expression of hepatocyte markers, whereas it upregulated cholangiocyte markers (Fig. 3C). Ad-TGFBR2 transduction decreased the percentage of ASGR1-positive hepatocyte-like cells but increased the percentage of AQP1-positive cholangiocyte-like cells (Fig. 3D). These results suggest that TGFBR2 overexpression inhibits hepatocyte differentiation, whereas it promotes cholangiocyte differentiation. Taken together, these results suggest that TGFBR2 plays an important role in deciding the differentiation lineage of HBCs.

To investigate whether hepatoblasts would undergo differentiation in a TGFBR2-associated manner *in vivo*, HBCs transfected/transduced with si-control, si-TGFBR2, Ad-LacZ or Ad-

Development (2014) doi:10.1242/dev.103168

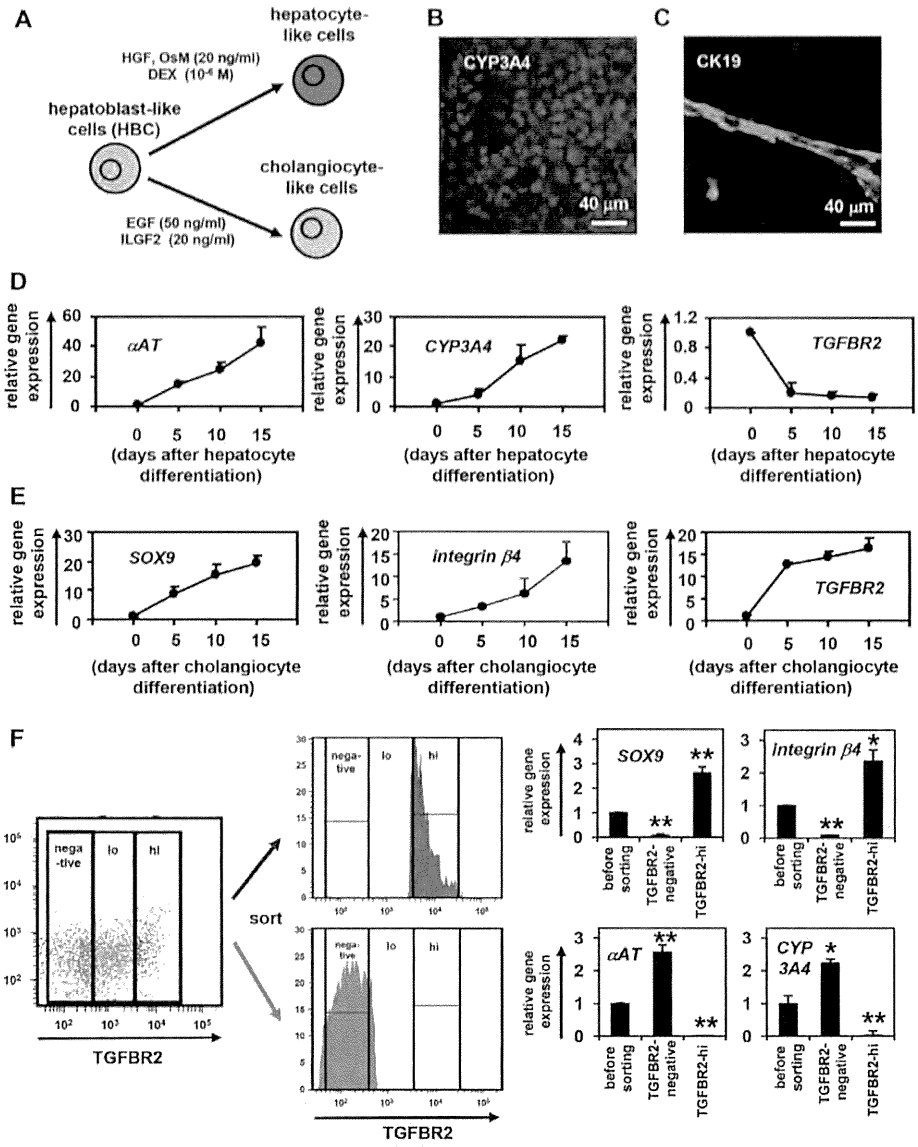

Fig. 1. HBCs can differentiate into both hepatocyte and cholangiocyte lineages. (A) The strategy for hepatocyte and cholangiocyte differentiation from HBCs. (B,C) The HBC-derived hepatocyte-like cells or cholangiocyte-like cells were subjected to immunostaining with anti-CYP3A4 (red, B) or anti-CK19 (green, C) antibodies, respectively. (D,E) Temporal gene expression levels of hepatocyte markers (*αAT* and *CYP3A4*) (D) or cholangiocyte markers (*SOX9* and integrin β4) (E) during hepatocyte or cholangiocyte differentiation as measured by real-time RT-PCR. The temporal gene expression of *TGFBR2* was also examined. The gene expression levels in HBCs were taken as 1.0. (F) HBCs were cultured on Matrigel for 5 days, and then the expression level of TGFBR2 was examined by FACS analysis. TGFBR2-negative, -lo and -hi populations were collected and real-time RT-PCR analysis was performed to measure the expression levels of hepatocyte markers (*αAT* and *CYP3A4*) and cholangiocyte markers (*SOX9* and integrin β4). $^{*}P<0.05$, $^{**}P<0.01$ (compared with 'before sorting'). Error bars indicate s.d. Statistical analysis was performed using the unpaired two-tailed Student's *t*-test ($n=3$).

TGFBR2 were transplanted into CCl_4-treated immunodeficient mice (Fig. 3E,F). Although some of the si-control-transfected or Ad-LacZ-transduced HBCs remained as HBCs (HNF4α and CK19 double positive), most of them showed *in vitro* differentiation toward hepatocyte-like cells (HNF4α single positive) (Fig. 3E, top row). By contrast, Ad-TGFBR2-transduced HBCs were predominantly committed to cholangiocyte-like cells (CK19 single positive) and si-TGFBR2-transfected HBCs were predominantly committed to hepatocyte-like cells (HNF4α single positive) (Fig. 3E, bottom row). Ad-TGFBR2 transduction decreased the percentage of HNF4α-positive hepatocyte-like cells, whereas it increased the percentage of CK19-positive cholangiocyte-like cells (supplementary material Fig. S5). The hepatocyte functionality of the *in vivo* differentiated HBCs was assessed by measuring secreted human ALB levels in the recipient mice (Fig. 3F). Mice that were transplanted with Ad-TGFBR2-transduced HBCs showed lower human ALB serum levels than those transplanted with Ad-LacZ-transduced HBCs, and the mice that were transplanted with si-TGFBR2-transfected HBCs showed higher human ALB serum levels than those transplanted with si-control-transfected HBCs. These data suggest that cholangiocyte or hepatocyte differentiation was promoted by TGFBR2 overexpression or knockdown, respectively. Thus, based on these data from *in vitro* and *in vivo* experiments, TGFBR2 plays an important role in deciding the differentiation lineage of HBCs.

TGFBR2 promoter activity and expression are negatively regulated by c/EBPα and positively regulated by c/EBPβ

A previous study has shown that TGFBR2 expression is upregulated in *Hnf6* knockout mice (Clotman et al., 2005), although we confirmed by ChIP assay that HNF6 does not bind to the *TGFBR2* promoter region (data not shown). Because c/EBPα is important in the hepatoblast fate decision (Suzuki et al., 2003), we expected that c/EBPs might directly regulate TGFBR2 expression. The *TGFBR2* promoter region was analyzed to examine whether TGFBR2 expression is regulated by c/EBPs. Some c/EBP binding sites (supplementary material Fig. S6) were predicted by rVista 2.0 (http://rvista.dcode.org/) (Fig. 4A). By performing a ChIP assay, one

Development (2014) doi:10.1242/dev.103168

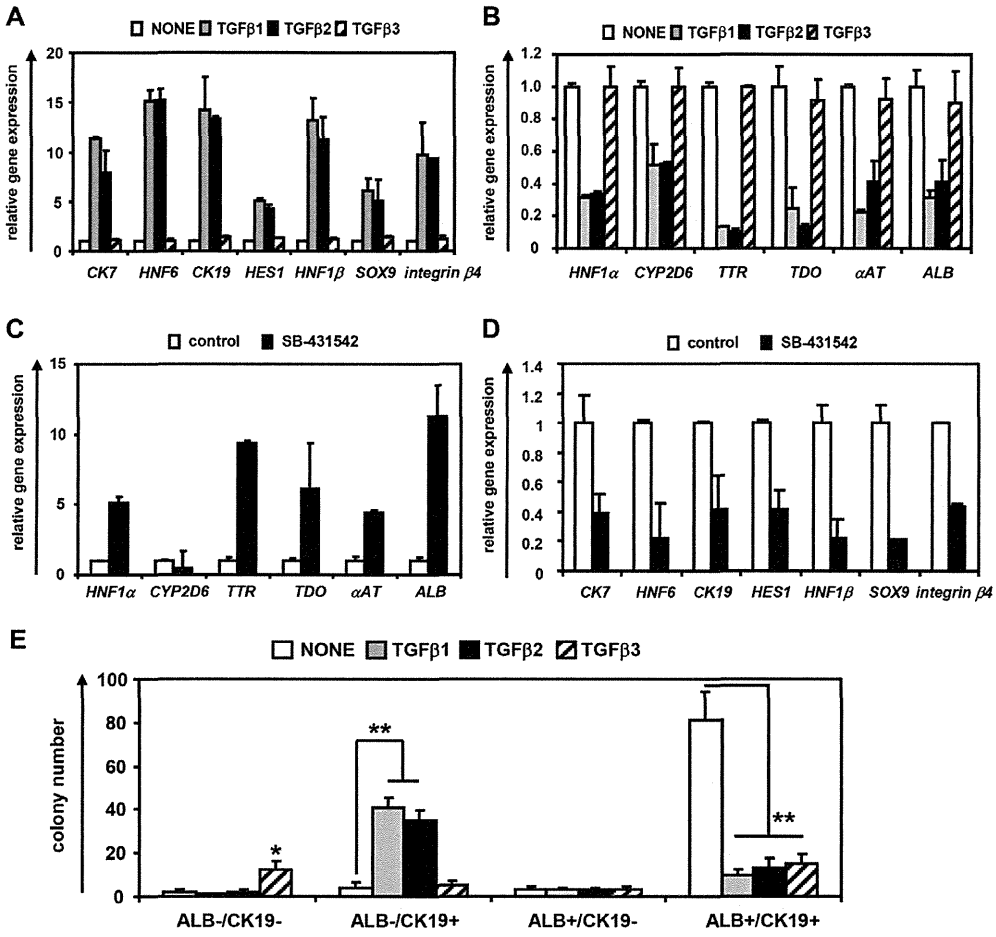

Fig. 2. Hepatocyte and cholangiocyte differentiation from HBCs is regulated by TGFβ signaling. (A,B) HBCs were cultured in differentiation hESF-DIF medium containing 10 ng/ml TGFβ1, TGFβ2 or TGFβ3 for 10 days. The expression levels of cholangiocyte (A) and hepatocyte (B) marker genes were measured by real-time RT-PCR. On the *y*-axis, the gene expression level of cholangiocyte markers in untreated cells (NONE) was taken as 1.0. (C,D) HBCs were cultured in differentiation hESF-DIF medium containing SB-431542 (10 μM) for 10 days. Control cells were treated with solvent only (0.1% DMSO). Expression levels of hepatocyte (C) and cholangiocyte (D) marker genes were measured by real-time RT-PCR. On the *y*-axis, the gene expression level of hepatocyte markers in untreated cells (control) was taken as 1.0. (E) HBC colony formation assay in the presence or absence of 10 ng/ml TGFβ1, TGFβ2 or TGFβ3. HBCs were plated at 200 cells/cm^2 on human LN111-coated dishes. The colonies were separated into four groups based on the expression of ALB and CK19: double-negative, ALB negative and CK19 positive, ALB positive and CK19 negative, and double positive. The numbers represent wells in which the colony was observed in three 96-well plates (total 288 wells). Five days after plating, the cells were fixed with 4% PFA and used for double immunostaining. **P*<0.05, ***P*<0.01 (compared with NONE). Error bars indicate s.d. Statistical analysis was performed using the unpaired two-tailed Student's *t*-test (*n*=3).

c/EBP binding site was found in the *TGFBR2* promoter region (Fig. 4B). A reporter assay of the *TGFBR2* promoter region showed that c/EBPβ activates *TGFBR2* promoter activity, whereas c/EBPα inhibits it (Fig. 4C). In addition, *TGFBR2* expression was downregulated by Ad-c/EBPα transduction, whereas *TGFBR2* was upregulated by Ad-c/EBPβ transduction in HepG2 cells (TGFBR2 positive) (Fig. 4D). We ascertained the expression of *c/EBPα* or *c/EBPβ* (*CEBPA* or *CEBPB* – Human Gene Nomenclature Committee) in the Ad-c/EBPα- or Ad-c/EBPβ-transduced cells, respectively (supplementary material Fig. S4). These results demonstrated that the promoter activity and expression of *TGFBR2* were directly regulated by both c/EBPα and c/EBPβ.

c/EBPs determine the cell fate decision of HBCs via regulation of TGFBR2 expression

To elucidate the relationship between TGFBR2 and c/EBPs (c/EBPα and c/EBPβ) in the hepatoblast fate decision, we first examined the temporal gene expression patterns of *TGFBR2*, *c/EBPα* and *c/EBPβ* in hepatocyte and cholangiocyte differentiation. During hepatocyte differentiation, *TGFBR2* expression was downregulated, whereas *c/EBPα* was upregulated (supplementary material Fig. S7A, top). During cholangiocyte differentiation, *c/EBPα* was downregulated, whereas *TGFBR2* and *c/EBPβ* were upregulated (supplementary material Fig. S7A, bottom). In addition, the ratio of *c/EBPα* to *c/EBPβ* was significantly increased in hepatocyte differentiation, but significantly reduced in cholangiocyte differentiation (supplementary material Fig. S7B). High-level expression of *c/EBPα* was detected in TGFBR2-negative cells, but not in TGFBR2-hi cells (supplementary material Fig. S7C). By contrast, high-level expression of *c/EBPβ* was detected in TGFBR2-hi cells, but not in TGFBR2-negative cells. These results suggest that TGFBR2 is negatively regulated by c/EBPα and positively regulated by c/EBPβ in the differentiation model from HBCs as well as in the HepG2 cell line (Fig. 4).

Development (2014) doi:10.1242/dev.103168

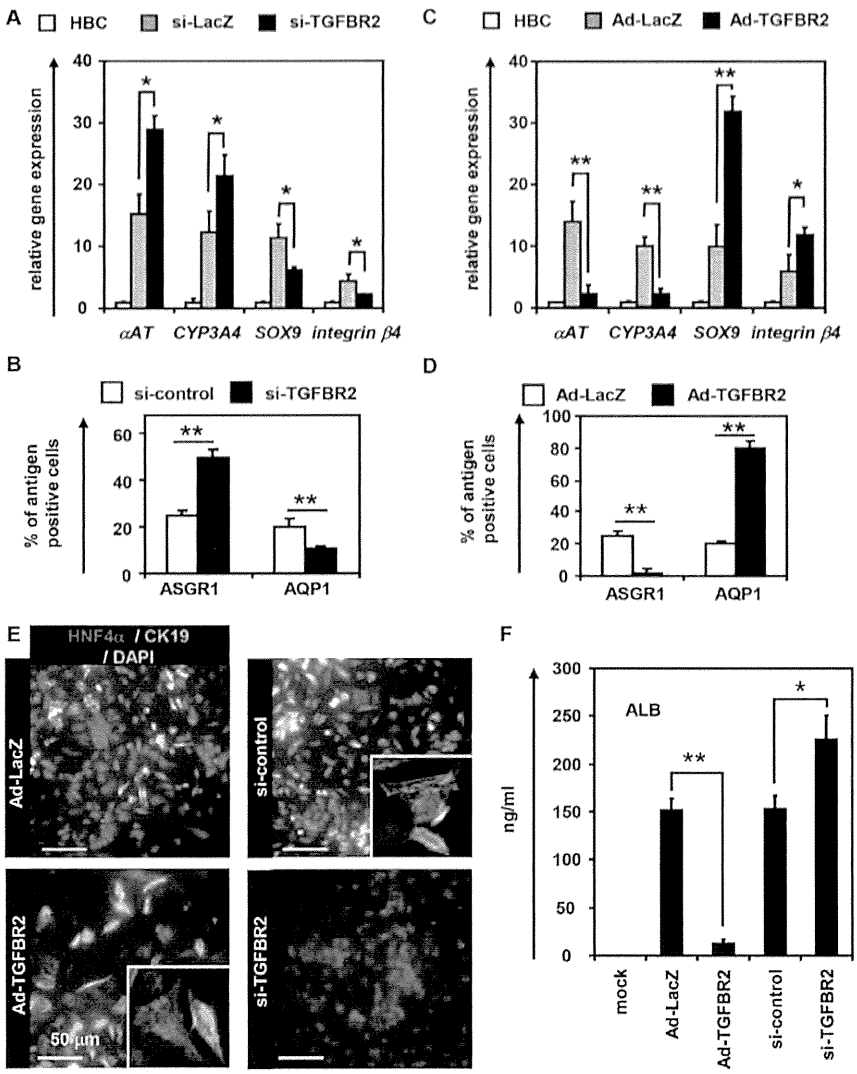

Fig. 3. TGFBR2 regulates bi-directional differentiation of HBCs. (A) HBCs were transfected with 50 nM control siRNA (si-control) or TGFBR2-suppressing siRNA (si-TGFBR2) and cultured in differentiation hESF-DIF medium for 10 days. The expression levels of hepatocyte (*αAT* and *CYP3A4*) or cholangiocyte (*SOX9* and integrin β4) markers were measured by real-time RT-PCR. On the *y*-axis, the gene expression level in HBCs was taken as 1.0. (B) On day 10 after siRNA transfection, the efficiency of hepatocyte or cholangiocyte differentiation was measured by estimating the percentage of ASGR1-positive or AQP1-positive cells, respectively, by FACS analysis. (C) HBCs were transduced with 3000 VPs/cell of Ad-LacZ or Ad-TGFBR2 for 1.5 hours and cultured in differentiation hESF-DIF medium for 10 days. Expression levels of hepatocyte or cholangiocyte marker genes were measured by real-time RT-PCR. On the *y*-axis, gene expression levels in the HBCs was taken as 1.0. (D) On day 10 after Ad vector transduction, the efficiency of hepatocyte or cholangiocyte differentiation was measured by estimating the percentage of ASGR1-positive or AQP1-positive cells, respectively, by FACS analysis. (E,F) The si-control, si-TGFBR2, Ad-LacZ- or Ad-TGFBR2-transfected/transduced HBCs (1.0×10^6 cells) were transplanted into CCl_4-treated (2 mg/kg) *Rag2/Il2rg* double-knockout mice by intrasplenic injection. (E) Expression of human HNF4α (red) and CK19 (green) was examined by double immunohistochemistry 2 weeks after transplantation. Nuclei were counterstained with DAPI (blue). (F) Levels of human ALB in recipient mouse serum were measured 2 weeks after transplantation. $^*P<0.05$, $^{**}P<0.01$ (compared with Ad-LacZ-transduced or si-control-transfected cells). Error bars indicate s.d. Statistical analysis was performed using the unpaired two-tailed Student's *t*-test ($n=3$).

ChIP experiments showed that c/EBPα or c/EBPβ is recruited to the *TGFBR2* promoter region containing the c/EBP binding site in hepatocyte-like cells or cholangiocyte-like cells, respectively (Fig. 5A), suggesting that c/EBPα and c/EBPβ oppositely regulate *TGFBR2* promoter activity in the differentiation from HBCs. We confirmed that c/EBPα or c/EBPβ was mainly recruited to the *TGFBR2* promoter region containing the c/EBP binding site in TGFBR-negative or TGFBR2-positive cells, respectively (supplementary material Fig. S7D). Taken together, we concluded that c/EBPα and c/EBPβ are able to regulate the cell fate decision of HBCs via regulation of TGFBR2 expression. During differentiation from HBCs, *TGFBR2* expression was negatively regulated by c/EBPα and positively regulated by c/EBPβ (Fig. 5B). To examine whether c/EBPα or c/EBPβ could regulate the differentiation from HBCs, *in vitro* gain- and loss-of-function analyses were performed. si-c/EBPα transfection downregulated hepatocyte marker gene expression, whereas it upregulated cholangiocyte marker genes (Fig. 5C). By contrast, si-c/EBPβ transfection upregulated hepatocyte marker and downregulated cholangiocyte marker gene expression (Fig. 5C). In accordance, Ad-c/EBPα transduction upregulated hepatocyte marker genes and downregulated cholangiocyte markers (Fig. 5D), whereas Ad-c/EBPβ transduction downregulated hepatocyte markers and upregulated cholangiocyte marker genes. Promotion of hepatocyte differentiation by Ad-c/EBPα transduction was inhibited by Ad-TGFBR2 transduction, whereas inhibition of cholangiocyte differentiation by Ad-c/EBPα transduction was rescued by Ad-TGFBR2 transduction (Fig. 5E). In addition, promotion of hepatocyte differentiation by si-c/EBPβ transfection was inhibited by Ad-TGFBR2 transduction, whereas inhibition of cholangiocyte differentiation by si-c/EBPβ transfection was rescued by Ad-TGFBR2 transduction (Fig. 5F). We further confirmed that inhibition of hepatocyte differentiation by si-c/EBPα-transfection was rescued by si-TGFBR2 transfection (supplementary material Fig. S8). Taken together, these results led us to conclude that c/EBPα and c/EBPβ could determine the cell fate of HBCs by negatively and positively regulating TGFBR2 expression, respectively (supplementary material Fig. S9).

c/EBPs organize the differentiation of fetal mouse hepatoblasts through regulation of TGFBR2 expression

We have demonstrated that c/EBPs may determine the HBC fate decision via regulation of the expression level of TGFBR2. To examine whether our findings could be replicated in native liver

Development (2014) doi:10.1242/dev.103168

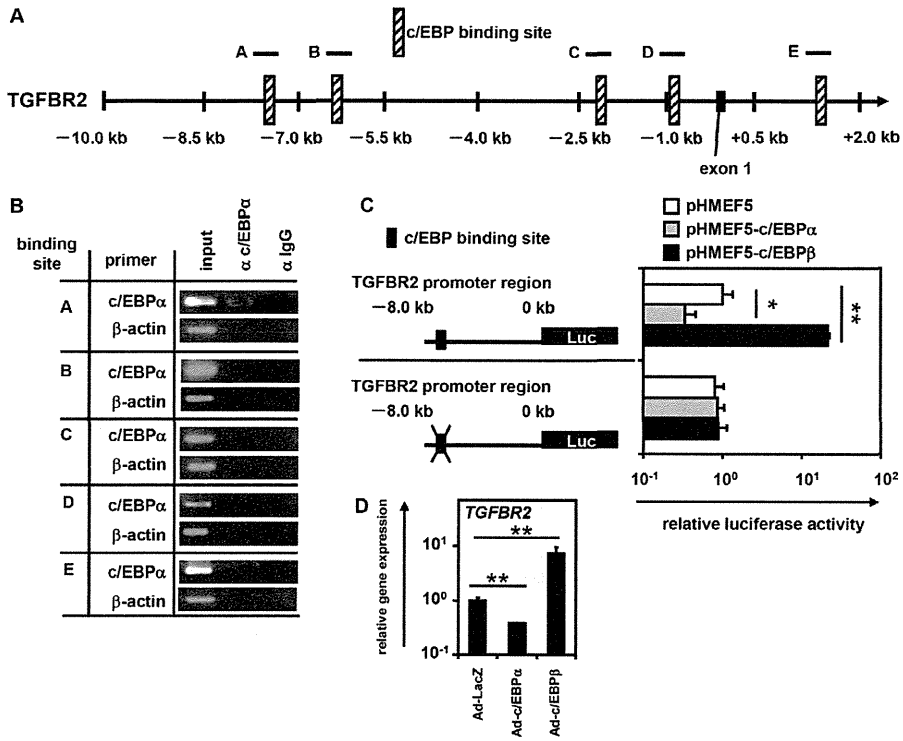

Fig. 4. *TGFBR2* promoter activity and expression are negatively regulated by c/EBPα and positively regulated by c/EBPβ. (A) Candidate c/EBP binding sites (hatched boxes) in the *TGFBR2* promoter region as predicted using rVista 2.0 (see supplementary material Fig. S7). (B) hESCs (H9 cells) were differentiated into hepatoblasts and then a ChIP assay performed. The antibodies and primers employed are summarized in supplementary material Tables S1 and S4. (C) HEK293 cells were transfected with firefly luciferase (Luc) expression plasmids containing the promoter region of *TGFBR2*. In addition, empty plasmid (pHMEF5), c/EBPα expression plasmid (pHMEF5-c/EBPα) or c/EBPβ expression plasmid (pHMEF5-c/EBPβ) was transfected. After 36 hours, a dual luciferase assay was performed. Base pair positions are relative to the translation start site (+1). (D) HepG2 cells (TGFBR2-positive cells) were transduced with 3000 VPs/cell of Ad-LacZ, Ad-c/EBPα or Ad-c/EBPβ for 1.5 hours and cultured for 48 hours. The expression level of *TGFBR2* in HepG2 cells was measured by real-time RT-PCR. On the *y*-axis, the gene expression level in Ad-LacZ-transduced cells was taken as 1.0. $^{*}P<0.05$, $^{**}P<0.01$. Error bars indicate s.d. Statistical analysis was performed using the unpaired two-tailed Student's *t*-test ($n=3$).

development, fetal hepatoblasts were purified from E13.5 mice. The gene expression level of *TGFBR2* in fetal mouse hepatoblasts was negatively or positively regulated by c/EBPα or c/EBPβ, respectively (Fig. 6A,B). The promotion of hepatocyte differentiation by Ad-c/EBPα transduction was inhibited by Ad-TGFBR2 transduction, whereas the inhibition of cholangiocyte differentiation by Ad-c/EBPα transduction was rescued by Ad-TGFBR2 transduction (Fig. 6C). In addition, the promotion of hepatocyte differentiation by si-c/EBPβ transfection was inhibited by Ad-TGFBR2 transduction, whereas the inhibition of cholangiocyte differentiation by si-c/EBPβ transfection was rescued by Ad-TGFBR2 transduction (Fig. 6D). Taken together, these results led us to conclude that c/EBPα and c/EBPβ could determine the cell fate of fetal mouse hepatoblasts by negatively and positively regulating TGFBR2 expression, respectively. Our *in vitro* differentiation system could also prove useful in elucidating the molecular mechanisms of human liver development.

DISCUSSION

The purpose of this study was to better understand the molecular mechanisms of the hepatoblast fate decision in humans. To elucidate the molecular mechanisms of liver development, both conditional knockout mouse models and cell culture systems are useful. For example, DeLaForest et al. demonstrated the role of HNF4α in hepatocyte differentiation using hESC culture systems (DeLaForest et al., 2011). The technology for inducing hepatocyte differentiation from hESCs has recently been dramatically advanced (Takayama et al., 2012a). Because it is possible to generate functional HBCs from hESCs, which can self-replicate and differentiate into both hepatocyte and cholangiocyte lineages (supplementary material Fig. S1 and Fig. 1), the differentiation model of HBCs generated from hESCs should provide a powerful tool for analyzing the molecular mechanisms of human liver development.

In this study, the molecular mechanisms of the hepatoblast fate decision were elucidated using hESC culture systems. HBCs cultured on human LN111 expressed hepatoblast markers (supplementary material Fig. S1) and had the ability to differentiate into both hepatocyte-like cells and cholangiocyte-like cells (Fig. 1). Because a previous study showed that low and high concentrations of TGFβ were required for hepatocyte and cholangiocyte differentiation, respectively (Clotman et al., 2005), we expected that TGFBR2 might contribute to the hepatoblast fate decision. Although TGFβ1, β2 and β3 are all ligands of TGFBR2, TGFβ3 did not promote cholangiocyte differentiation (Fig. 2). This might have been because only TGFβ3 is unable to upregulate the expression of *SOX9*, which is the key factor in bile duct development *in vivo* and cholangiocyte differentiation *in vitro* (Antoniou et al., 2009). We examined the function of TGFBR2 in the hepatoblast fate decision, and found that its overexpression promoted cholangiocyte differentiation, whereas TGFBR2 knockdown promoted hepatocyte differentiation (Fig. 3). Although an exogenous TGFβ ligand was not added to the differentiation medium, the endogenous TGFβ ligand present in Matrigel, which was used in our differentiation protocol, might have bound to TGFBR2. It might also be that the cells committed to the biliary lineage express TGFβ, as a previous study showed that bile duct epithelial cells express TGFβ (Lewindon et al., 2002).

To examine the molecular mechanism regulating TGFBR2 expression, the *TGFBR2* promoter region was analyzed (Fig. 4). *TGFBR2* promoter activity was negatively regulated by c/EBPα and positively regulated by c/EBPβ. c/EBPα overexpression downregulated *TGFBR2* promoter activity in spite of the fact that c/EBPα protein has no repression domain (Yoshida et al., 2006). CTBP1 and CTBP2 (Vernochet et al., 2009) are known to be co-repressors of c/EBPα, and as such constitute candidate co-repressors recruited to the c/EBP binding site in the *TGFBR2* promoter region.

Development (2014) doi:10.1242/dev.103168

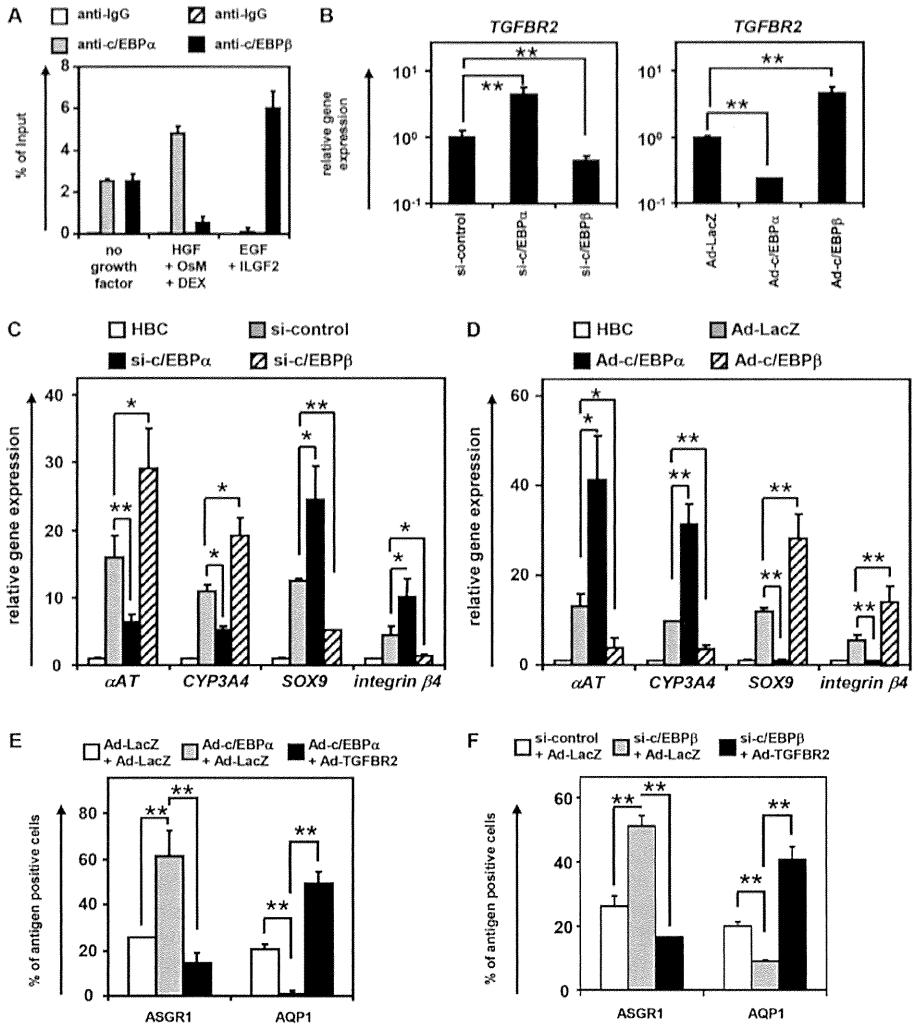

Fig. 5. c/EBPα and c/EBPβ promote hepatocyte and cholangiocyte differentiation by regulating *TGFBR2* expression, respectively. (A) HBCs were differentiated into hepatocyte-like cells or cholangiocyte-like cells according to the scheme outlined in Fig. 1A. On day 10 after hepatocyte or cholangiocyte differentiation, recruitment of c/EBPα or c/EBPβ to the *TGFBR2* promoter region was examined by ChIP assay. (B-D) HBCs were transfected with 50 nM si-control, si-c/EBPα or si-c/EBPβ and cultured in differentiation hESF-DIF medium for 10 days (B left, C). The expression levels of *TGFBR2* and hepatocyte and cholangiocyte markers were then measured by real-time RT-PCR. (B right, D) HBCs were transduced with 3000 VPs/cell of Ad-LacZ, Ad-c/EBPα or Ad-c/EBPβ for 1.5 hours and cultured in differentiation hESF-DIF medium for 10 days. The expression levels of *TGFBR2* and hepatocyte and cholangiocyte markers were then measured by real-time RT-PCR. On the *y*-axis, the gene expression level in the si-control-transfected or Ad-LacZ-transduced cells was taken as 1.0 in B, and levels in HBCs were taken as 1.0 in C and D. (E) HBCs were transduced with 3000 VPs/cell each of Ad-LacZ + Ad-LacZ, Ad-c/EBPα + Ad-LacZ, or Ad-c/EBPα + Ad-TGFBR2 for 1.5 hours and cultured in differentiation hESF-DIF medium for 10 days. The efficiency of hepatocyte or cholangiocyte differentiation was measured by estimating the percentage of ASGR1-positive or AQP1-positive cells, respectively, by FACS analysis. (F) HBCs were transduced with 3000 VPs/cell of Ad-LacZ or Ad-TGFBR2 and then transfected with 50 nM si-control or si-c/EBPβ and cultured in hESF-DIF medium for 10 days. The efficiency of hepatocyte or cholangiocyte differentiation was measured by estimating the percentage of ASGR1-positive or AQP1-positive cells, respectively, by FACS analysis. **P*<0.05, ***P*<0.01. Error bars indicate s.d. Statistical analysis was performed using the unpaired two-tailed Student's *t*-test (*n*=3).

Proteome analysis of c/EBPα would provide an opportunity to identify the co-repressor of c/EBPα. Because large numbers of nearly homogeneous hepatoblasts can be differentiated from hESCs, as compared with the isolation of fetal liver hepatoblasts, hepatocyte differentiation technology from hESCs might prove useful in proteome analysis.

We found that Ad-c/EBPα transduction could promote hepatocyte differentiation by suppressing TGFBR2 expression (Fig. 5). Our findings might thus provide a detailed explanation of the phenotype of *c/EBPα* knockout mice; that is, hepatocyte differentiation is inhibited and cholangiocyte differentiation is promoted in these mice (Yamasaki et al., 2006). We also found that Ad-c/EBPβ transduction could promote cholangiocyte differentiation by enhancing TGFBR2 expression. Because both c/EBPα and c/EBPβ can bind to the same binding site, reciprocal competition for binding is likely to be influenced by regulating c/EBPα or c/EBPβ expression. Therefore, the expression ratio between c/EBPα and c/EBPβ might determine the cell fate of hepatoblasts by regulating the expression level of TGFBR2. We confirmed that our findings could be reproduced in fetal mouse hepatoblasts (Fig. 6). Because a previous study had

Development (2014) doi:10.1242/dev.103168

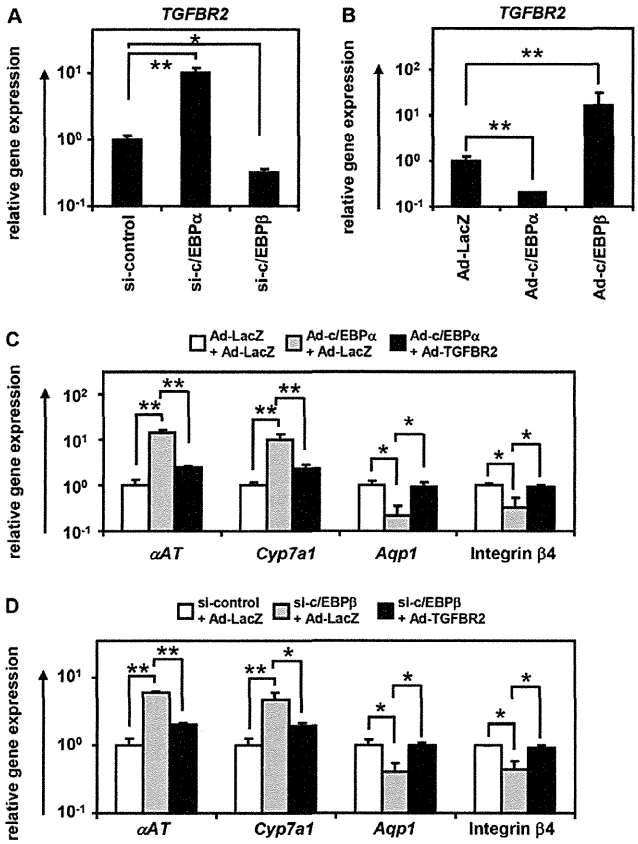

Fig. 6. c/EBPs control the differentiation of fetal mouse hepatoblasts through regulation of TGFBR2 expression. Fetal mouse hepatoblasts (Dlk1-positive cells; the purity was over 98%) were sorted from E13.5 mouse liver. (A) Fetal mouse hepatoblasts were transfected with 50 nM si-control, si-c/EBPα or si-c/EBPβ and cultured for 5 days. The expression of *TGFBR2* was measured by real-time RT-PCR. (B) Fetal mouse hepatoblasts were transduced with 3000 VPs/cell of Ad-LacZ, Ad-c/EBPα or Ad-c/EBPβ for 1.5 hours and cultured for 5 days. The expression of *TGFBR2* was measured by real-time RT-PCR. On the *y*-axis, the gene expression level in the si-control-transfected cells or Ad-LacZ-transduced cells was taken as 1.0. (C) Fetal mouse hepatoblasts were transduced with 3000 VPs/cell each of Ad-LacZ + Ad-LacZ, Ad-c/EBPα + Ad-LacZ, or Ad-c/EBPα + Ad-TGFBR2 for 1.5 hours and cultured for 5 days. On day 5, the expression levels of hepatocyte (*αAT* and *Cyp7a1*) and cholangiocyte (*Aqp1* and integrin β4) markers were measured by real-time RT-PCR. (D) Fetal mouse hepatoblasts were transduced with 3000 VPs/cell of Ad-LacZ or Ad-TGFBR2 and then transfected with 50 nM si-control or si-c/EBPβ and cultured for 5 days. On day 5, the gene levels of hepatocyte (*αAT* and *Cyp7a1*) and cholangiocyte (*Aqp1* and integrin β4) markers were measured by real-time RT-PCR. On the *y*-axis, the gene expression level in the si-control-transfected or Ad-LacZ-transduced cells was taken as 1.0. **P*<0.05, ***P*<0.01. Error bars indicate s.d. Statistical analysis was performed using the unpaired two-tailed Student's *t*-test (*n*=3).

shown that the addition of hepatocyte growth factor (HGF) to hepatoblasts upregulated the expression of c/EBPα and downregulated the expression of c/EBPβ (Suzuki et al., 2003), the ratio between c/EBPα and c/EBPβ might be determined by HGF during hepatocyte differentiation.

In this study, we have identified for the first time that *TGFBR2* is a target of c/EBPs in the hepatoblast fate decision (supplementary material Fig. S9). c/EBPα promotes hepatocyte differentiation by downregulating the expression of TGFBR2, whereas c/EBPβ promotes cholangiocyte differentiation by upregulating TGFBR2 expression. This study might have revealed a molecular mechanism underlying the lineage commitment of human hepatoblasts controlled by a gradient of TGFβ signaling. We believe that similar procedures that adopt the model of human pluripotent stem cell (including human iPS cell) differentiation will be used not only for the elucidation of molecular mechanisms underlying human hepatocyte and biliary differentiation but also for investigating the causes of congenital anomalies of the human liver and biliary tract.

MATERIALS AND METHODS

Ad vectors

Ad vectors were constructed by an improved *in vitro* ligation method (Mizuguchi and Kay, 1998; Mizuguchi and Kay, 1999). The human *c/EBPα* and *c/EBPβ* genes (accession numbers NM_004364 and NM_005194, respectively) were amplified by PCR using the following primers: c/EBPα, Fwd 5′-GCTCTAGATGCCGGGAGAACTCTAACTC-3′ and Rev 5′-GCGGTACCAAACCACTCCCTGGGTCC-3′; c/EBPβ, Fwd 5′-GCATCTAGATTCATGCAACGCCTGGTG-3′ and Rev 5′-ATAGGTACCTAAAATTACCGACGGGCTCC-3′. The human *TGFBR2* gene was purchased from Addgene (plasmid 16622). The human *c/EBPα*, *c/EBPβ* or *TGFBR2* gene was inserted into pBSKII (Invitrogen), resulting in pBSKII-c/EBPα, -c/EBPβ or -TGFBR2. Then, human *c/EBPα*, *c/EBPβ* or *TGFBR2* was inserted into pHMEF5 (Kawabata et al., 2005), which contains the human elongation factor 1α (*EF1α*, also known as *EEF1A1*) promoter, resulting in pHMEF5-c/EBPα, -c/EBPβ or -TGFBR2. pHMEF5-c/EBPα, -c/EBPβ or -TGFBR2 was digested with I-*Ceu*I/PI-*Sce*I and ligated into I-*Ceu*I/PI-*Sce*I-digested pAdHM41-K7 (Koizumi et al., 2003), resulting in pAd-c/EBPα, -c/EBPβ or -TGFBR2. The human *EF1α* promoter-driven *lacZ*- or FOXA2-expressing Ad vectors (Ad-LacZ or Ad-FOXA2, respectively) were constructed previously (Takayama et al., 2012b; Tashiro et al., 2008). All Ad vectors contain a stretch of lysine residues (K7) in the C-terminal region of the fiber knob for more efficient transduction of hESCs, definitive endoderm cells and HBCs, in which transfection efficiency was almost 100%, and the Ad vectors were purified as described previously (Takayama et al., 2012a; Takayama et al., 2011). The vector particle (VP) titer was determined by a spectrophotometric method (Maizel et al., 1968).

hESC culture

The H9 hESC line (WiCell Research Institute) was maintained on a feeder layer of mitomycin C-treated mouse embryonic fibroblasts (Merck Millipore) in ReproStem medium (ReproCELL) supplemented with 5 ng/ml FGF2 (Katayama Kagaku Kogyo). H9 was used following the Guidelines for Derivation and Utilization of Human Embryonic Stem Cells of the Ministry of Education, Culture, Sports, Science and Technology of Japan and the study was approved by the Independent Ethics Committee.

Generation and maintenance of hESC-derived HBCs

Before the initiation of cellular differentiation, the hESC medium was exchanged for a defined serum-free medium, hESF9, and cultured as previously reported (Furue et al., 2008). The differentiation protocol for the induction of definitive endoderm cells and HBCs was based on our previous reports with some modifications (Takayama et al., 2012a; Takayama et al., 2012b; Takayama et al., 2011). Briefly, in mesendoderm differentiation, hESCs were cultured for 2 days on Matrigel Matrix (BD Biosciences) in differentiation hESF-DIF medium, which contains 100 ng/ml activin A (R&D Systems); hESF-DIF medium was purchased from Cell Science & Technology Institute; differentiation hESF-DIF medium was supplemented with 10 μg/ml human recombinant insulin, 5 μg/ml human apotransferrin, 10 μM 2-mercaptoethanol, 10 μM ethanolamine, 10 μM sodium selenite, 0.5 mg/ml bovine fatty acid-free serum albumin (all from Sigma) and 1×B27 Supplement (without vitamin A; Invitrogen). To generate definitive endoderm cells, the mesendoderm cells were transduced with 3000 VPs/cell of FOXA2-expressing Ad vector (Ad-FOXA2) for 1.5 hours on day 2 and cultured until day 6 on Matrigel in differentiation hESF-DIF medium supplemented with 100 ng/ml activin A. For induction of the HBCs, the

definitive endoderm cells were cultured for 3 days on Matrigel in differentiation hESF-DIF medium supplemented with 20 ng/ml BMP4 (R&D Systems) and 20 ng/ml FGF4 (R&D Systems). Transient overexpression of FOXA2 in the mesendoderm cells is not necessary for establishing HBCs, but it is helpful for efficient generation of the HBCs. The HBCs were first purified from the hESC-derived cells (day 9) by selecting attached cells on a human recombinant LN111 (BioLamina)-coated dish 15 minutes after plating (Takayama et al., 2013). The HBCs were cultured on a human LN111-coated dish (2.0×10^4 cells/cm^2) in maintenance DMEM/F12 medium [DMEM/F12 medium (Invitrogen) supplemented with 10% fetal bovine serum (FBS), 1× insulin/transferrin/selenium, 10 mM nicotinamide, 0.1 μM dexamethasone (DEX) (Sigma), 20 mM HEPES, 25 mM $NaHCO_3$, 2 mM L-glutamine, and penicillin/streptomycin] which contained 40 ng/ml HGF (R&D Systems) and 20 ng/ml epidermal growth factors (EGF) (R&D Systems). The medium was refreshed every day. The HBCs were dissociated with Accutase (Millipore) into single cells, and subcultured every 6 or 7 days. The HBCs used in this study were passaged more than three times.

In vitro hepatocyte and cholangiocyte differentiation

To induce hepatocyte differentiation, the HBCs were cultured on a Matrigel-coated dish (7.5×10^4 cells/cm^2) in Hepatocyte Culture Medium (HCM without EGF; Lonza) supplemented with 20 ng/ml HGF, 20 ng/ml Oncostatin M (OsM) (R&D Systems) and 1 μM DEX. To induce cholangiocyte differentiation, the HBCs were cultured in collagen gel. To establish collagen gel plates, 500 μl collagen gel solution [400 μl type I-A collagen (Nitta gelatin), 50 μl 10× DMEM and 50 μl 200 mM HEPES buffer containing 2.2% $NaHCO_3$ and 0.05 M NaOH] was added to each well, and then the plates were incubated at 37°C for 30 minutes. The HBCs (5×10^4 cells) were resuspended in 500 μl differentiation DMEM/F12 medium [DMEM/F12 medium supplemented with 20 mM HEPES, 2 mM L-glutamine, 100 ng/ml EGF and 40 ng/ml ILGF2 (IGF2)], and then mixed with 500 μl of the collagen gel solution and plated onto the basal layer of collagen. After 30 minutes, 2 ml differentiation DMEM/F12 medium was added to the well.

Inhibition of TGFβ signaling

SB-431542 (Santa Cruz Biotechnology), which is a small molecule that acts as a selective inhibitor of activin receptor-like kinase (ALK) receptors [ALK4, ALK5 and ALK7 (also known as ACVR1B, TGFBR1 and ACVR1C)], was used to inhibit TGFβ signaling in HBCs.

Flow cytometry

Single-cell suspensions of hESC-derived cells were fixed with 2% paraformaldehyde (PFA) at 4°C for 20 minutes, and then incubated with primary antibody (supplementary material Table S1) followed by secondary antibody (supplementary material Table S2). Flow cytometry analysis was performed using a FACS LSR Fortessa flow cytometer (BD Biosciences). Cell sorting was performed using a FACS Aria (BD Biosciences).

RNA isolation and reverse transcription (RT)-PCR

Total RNA was isolated from hESCs and their derivatives using ISOGENE (Nippon Gene). cDNA was synthesized using 500 ng total RNA with the SuperScript VILO cDNA Synthesis Kit (Invitrogen). Real-time RT-PCR was performed with SYBR Green PCR Master Mix (Applied Biosystems) using an Applied Biosystems StemOnePlus real-time PCR system. Relative quantification was performed against a standard curve and the values were normalized against the input determined for the housekeeping gene *GAPDH*. Primers are described in supplementary material Table S3.

Immunohistochemistry

Cells were fixed with 4% PFA. After incubation with 0.1% Triton X-100 (Wako), blocking with Blocking One (Nakalai Tesque) or PBS containing 2% FBS, 2% BSA and 0.1% Triton X-100, the cells were incubated with primary antibody (supplementary material Table S1) at 4°C overnight, followed by secondary antibody (supplementary material Table S2) at room temperature for 1 hour. Immunopositive cells were counted in at least eight randomly chosen fields.

HBC colony formation assay

For the colony formation assay, HBCs were cultured at a low density (200 cells/cm^2) on a human LN111-coated dish in maintenance DMEM/F12 medium supplemented with 25 μM LY-27632 (ROCK inhibitor; Millipore).

Transplantation of clonally derived HBCs

Clonally derived HBCs were dissociated using Accutase and then suspended in maintenance DMEM/F12 medium without serum. The HBCs (1×10^6 cells) were transplanted 24 hours after administration of CCl_4 (2 mg/kg) by intrasplenic injection into 8- to 10-week-old *Rag2/Il2rg* double-knockout mice. Recipient mouse livers and blood were harvested 2 weeks after transplantation. Grafts were fixed with 4% PFA and processed for immunohistochemistry. Serum was extracted and subjected to ELISA. All animal experiments were conducted in accordance with institutional guidelines.

ELISA

Levels of human ALB in mouse serum were examined by ELISA using kits from Bethyl Laboratories according to the manufacturer's instructions.

Culture of mouse Dlk1$^+$ cells

Dlk1$^+$ hepatoblasts were isolated from E13.5 mouse livers using anti-mouse Dlk1 monoclonal antibody (MBL International Corporation, D187-4) as described previously (Tanimizu et al., 2003). Dlk1$^+$ cells were resuspended in DMEM/F12 (Sigma) containing 10% FBS, 1× insulin/transferrin/selenium (ITS), 10 mM nicotinamide (Wako), 0.1 μM DEX and 5 mM L-glutamine. Cells were plated on laminin-coated dishes and cultured in medium containing 20 ng/ml HGF, EGF and 25 μM LY-27632 (ROCK inhibitor).

lacZ assay

Hepatoblasts were transduced with Ad-LacZ at 3000 VPs/cell for 1.5 hours. The day after transduction (day 10), 5-bromo-4-chloro-3-indolyl β-D-galactopyranoside (X-Gal) staining was performed as described previously (Kawabata et al., 2005).

Reporter assays

The effects of c/EBPα or c/EBPβ overexpression on *TGFBR2* promoter activity were examined using a reporter assay. An 8 kb fragment of the 5′ flanking region of the *TGFBR2* gene was amplified by PCR using the following primers: Fwd, 5′-CCGAGCTCATGTTTGATGAAGTGTCTAG-CTTCCAAGG-3′; Rev, 5′-GGCTCGAGCCTCGACGTCCAGCCCCT-3′. The fragment was inserted into the *Sac*I/*Xho*I sites of pGL3-basic (Promega), resulting in a pGL3-*TGFBR2* promoter region (pGL3-TGFBR2-PR). To generate a *TGFBR2* promoter region containing mutations in the c/EBP binding site, the following primers were used in PCR (mutations are indicated by lowercase letters): Fwd, 5′-CACTAGTATTCAgTG-AtCcgAAAATATGG-3′; Rev, 5′-CACTAGTATTCAgTGAtCcgAAAA-TATGG-3′; this resulted in pGL3-mTGFBR2-PR. HEK293 cells were maintained in DMEM (Wako) supplemented with 10% FBS, penicillin and streptomycin, and 2 mM L-glutamine. In reporter assays, 60 ng pGL3-TGFBR2-PR or pGL3-mTGFBR2-PR was transfected together with 720 ng each expression plasmid (pHMEF5, pHMEF5-c/EBPα and pHMEF5-c/EBPβ) and 60 ng internal control plasmid (pCMV-Renilla luciferase) using Lipofectamine 2000 reagent (Invitrogen). Transfected cells were cultured for 36 hours, and a Dual Luciferase Assay (Promega) was performed according to the manufacturer's instructions.

siRNA-mediated knockdown

Predesigned siRNAs targeting *c/EBPα*, *c/EBPβ* and *TGFBR2* mRNAs were purchased from Thermo Scientific Dharmacon. Cells were transfected with 50 nM siRNA using RNAiMAX (Invitrogen) transfection reagent according to the manufacturer's instructions. As a negative control, we used scrambled siRNA (Qiagen) of a sequence showing no significant similarity to any mammalian gene.

Chromatin immunoprecipitation (ChIP) assay

The ChIP assay kit was purchased from Upstate. Cells were crosslinked using formaldehyde at a final concentration of 1% at 37°C for 10 minutes, and then genomic DNA was fragmented by sonicator. The resulting DNA-protein complexes were immunoprecipitated using the antibodies described in supplementary material Table S1 or control IgG as described in supplementary material Table S2. The precipitated DNA fragments were analyzed by real-time RT-PCR using the primers shown in supplementary material Table S4 to amplify the *TGFBR2* promoter region including the c/EBP binding sites or β-actin locus as a control. The results of quantitative ChIP analysis (Fig. 5A) were expressed as the amount of amplified *TGFBR2* promoter region relative to input DNA taken as 100%.

Statistical analysis

Statistical analysis was performed using an unpaired two-tailed Student's *t*-test. All data are represented as mean ± s.d. (n=3).

Acknowledgements

We thank Natsumi Mimura, Yasuko Hagihara and Hiroko Matsumura for excellent technical support.

Competing interests

The authors declare no competing financial interests.

Author contributions

K. Takayama, K.K. and H.M. developed the concepts or approach; K. Takayama, Y.N., K.O., H.O. and T.Y. performed experiments; K. Takayama, K.K., M.I., K. Tashiro, F.S., T.H., T.O., M.F.K. and H.M. performed data analysis; K. Takayama, K.K. and H.M. prepared or edited the manuscript prior to submission.

Funding

H.M., K.K., M.K.F. and T.H. were supported by grants from the Ministry of Health, Labor, and Welfare of Japan (MEXT). H.M. was also supported by Japan Research Foundation for Clinical Pharmacology, The Uehara Memorial Foundation. K.O. was supported by Special Coordination Funds for Promoting Science and Technology from MEXT. F.S. was supported by Program for Promotion of Fundamental Studies in Health Sciences of the National Institute of Biomedical Innovation (NIBIO). K. Takayama and Y.N. are Research Fellows of the Japan Society for the Promotion of Science.

Supplementary material

Supplementary material available online at
http://dev.biologists.org/lookup/suppl/doi:10.1242/dev.103168/-/DC1

References

Agarwal, S., Holton, K. L. and Lanza, R. (2008). Efficient differentiation of functional hepatocytes from human embryonic stem cells. *Stem Cells* **26**, 1117-1127.

Antoniou, A., Raynaud, P., Cordi, S., Zong, Y., Tronche, F., Stanger, B. Z., Jacquemin, P., Pierreux, C. E., Clotman, F. and Lemaigre, F. P. (2009). Intrahepatic bile ducts develop according to a new mode of tubulogenesis regulated by the transcription factor SOX9. *Gastroenterology* **136**, 2325-2333.

Chen, S. S., Chen, J. F., Johnson, P. F., Muppala, V. and Lee, Y. H. (2000). C/EBPbeta, when expressed from the C/ebpalpha gene locus, can functionally replace C/EBPalpha in liver but not in adipose tissue. *Mol. Cell. Biol.* **20**, 7292-7299.

Clotman, F., Jacquemin, P., Plumb-Rudewiez, N., Pierreux, C. E., Van der Smissen, P., Dietz, H. C., Courtoy, P. J., Rousseau, G. G. and Lemaigre, F. P. (2005). Control of liver cell fate decision by a gradient of TGF beta signaling modulated by Onecut transcription factors. *Genes Dev.* **19**, 1849-1854.

DeLaForest, A., Nagaoka, M., Si-Tayeb, K., Noto, F. K., Konopka, G., Battle, M. A. and Duncan, S. A. (2011). HNF4A is essential for specification of hepatic progenitors from human pluripotent stem cells. *Development* **138**, 4143-4153.

Furue, M. K., Na, J., Jackson, J. P., Okamoto, T., Jones, M., Baker, D., Hata, R., Moore, H. D., Sato, J. D. and Andrews, P. W. (2008). Heparin promotes the growth of human embryonic stem cells in a defined serum-free medium. *Proc. Natl. Acad. Sci. USA* **105**, 13409-13414.

Hansen, A. J., Lee, Y. H., Sterneck, E., Gonzalez, F. J. and Mackenzie, P. I. (1998). C/EBPalpha is a regulator of the UDP glucuronosyltransferase UGT2B1 gene. *Mol. Pharmacol.* **53**, 1027-1033.

Kawabata, K., Sakurai, F., Yamaguchi, T., Hayakawa, T. and Mizuguchi, H. (2005). Efficient gene transfer into mouse embryonic stem cells with adenovirus vectors. *Mol. Ther.* **12**, 547-554.

Kitisin, K., Saha, T., Blake, T., Golestaneh, N., Deng, M., Kim, C., Tang, Y., Shetty, K., Mishra, B. and Mishra, L. (2007). Tgf-Beta signaling in development. *Sci. STKE* **2007**, cm1.

Koizumi, N., Mizuguchi, H., Utoguchi, N., Watanabe, Y. and Hayakawa, T. (2003). Generation of fiber-modified adenovirus vectors containing heterologous peptides in both the HI loop and C terminus of the fiber knob. *J. Gene Med.* **5**, 267-276.

Lewindon, P. J., Pereira, T. N., Hoskins, A. C., Bridle, K. R., Williamson, R. M., Shepherd, R. W. and Ramm, G. A. (2002). The role of hepatic stellate cells and transforming growth factor-beta(1) in cystic fibrosis liver disease. *Am. J. Pathol.* **160**, 1705-1715.

Maizel, J. V., Jr, White, D. O. and Scharff, M. D. (1968). The polypeptides of adenovirus. I. Evidence for multiple protein components in the virion and a comparison of types 2, 7A, and 12. *Virology* **36**, 115-125.

Mizuguchi, H. and Kay, M. A. (1998). Efficient construction of a recombinant adenovirus vector by an improved in vitro ligation method. *Hum. Gene Ther.* **9**, 2577-2583.

Mizuguchi, H. and Kay, M. A. (1999). A simple method for constructing E1- and E1/E4-deleted recombinant adenoviral vectors. *Hum. Gene Ther.* **10**, 2013-2017.

Oe, S., Lemmer, E. R., Conner, E. A., Factor, V. M., Levéen, P., Larsson, J., Karlsson, S. and Thorgeirsson, S. S. (2004). Intact signaling by transforming growth factor beta is not required for termination of liver regeneration in mice. *Hepatology* **40**, 1098-1105.

Plumb-Rudewiez, N., Clotman, F., Strick-Marchand, H., Pierreux, C. E., Weiss, M. C., Rousseau, G. G. and Lemaigre, F. P. (2004). Transcription factor HNF-6/OC-1 inhibits the stimulation of the HNF-3alpha/Foxa1 gene by TGF-beta in mouse liver. *Hepatology* **40**, 1266-1274.

Schmelzer, E., Zhang, L., Bruce, A., Wauthier, E., Ludlow, J., Yao, H. L., Moss, N., Melhem, A., McClelland, R., Turner, W. et al. (2007). Human hepatic stem cells from fetal and postnatal donors. *J. Exp. Med.* **204**, 1973-1987.

Suzuki, A., Iwama, A., Miyashita, H., Nakauchi, H. and Taniguchi, H. (2003). Role for growth factors and extracellular matrix in controlling differentiation of prospectively isolated hepatic stem cells. *Development* **130**, 2513-2524.

Takayama, K., Inamura, M., Kawabata, K., Tashiro, K., Katayama, K., Sakurai, F., Hayakawa, T., Furue, M. K. and Mizuguchi, H. (2011). Efficient and directive generation of two distinct endoderm lineages from human ESCs and iPSCs by differentiation stage-specific SOX17 transduction. *PLoS ONE* **6**, e21780.

Takayama, K., Inamura, M., Kawabata, K., Katayama, K., Higuchi, M., Tashiro, K., Nonaka, A., Sakurai, F., Hayakawa, T., Furue, M. K. et al. (2012a). Efficient generation of functional hepatocytes from human embryonic stem cells and induced pluripotent stem cells by HNF4α transduction. *Mol. Ther.* **20**, 127-137.

Takayama, K., Inamura, M., Kawabata, K., Sugawara, M., Kikuchi, K., Higuchi, M., Nagamoto, Y., Watanabe, H., Tashiro, K., Sakurai, F. et al. (2012b). Generation of metabolically functioning hepatocytes from human pluripotent stem cells by FOXA2 and HNF1α transduction. *J. Hepatol.* **57**, 628-636.

Takayama, K., Nagamoto, Y., Mimura, N., Tashiro, K., Sakurai, F., Tachibana, M., Hayakawa, T., Kawabata, K. and Mizuguchi, H. (2013). Long-term self-renewal of human ES/iPS-derived hepatoblast-like cells on human laminin 111-coated dishes. *Stem Cell Reports* **1**, 322-335.

Tanimizu, N., Nishikawa, M., Saito, H., Tsujimura, T. and Miyajima, A. (2003). Isolation of hepatoblasts based on the expression of Dlk/Pref-1. *J. Cell Sci.* **116**, 1775-1786.

Tashiro, K., Kawabata, K., Sakurai, H., Kurachi, S., Sakurai, F., Yamanishi, K. and Mizuguchi, H. (2008). Efficient adenovirus vector-mediated PPAR gamma gene transfer into mouse embryoid bodies promotes adipocyte differentiation. *J. Gene Med.* **10**, 498-507.

Tomizawa, M., Garfield, S., Factor, V. and Xanthopoulos, K. G. (1998). Hepatocytes deficient in CCAAT/enhancer binding protein alpha (C/EBP alpha) exhibit both hepatocyte and biliary epithelial cell character. *Biochem. Biophys. Res. Commun.* **249**, 1-5.

Vernochet, C., Peres, S. B., Davis, K. E., McDonald, M. E., Qiang, L., Wang, H., Scherer, P. E. and Farmer, S. R. (2009). C/EBPalpha and the corepressors CtBP1 and CtBP2 regulate repression of select visceral white adipose genes during induction of the brown phenotype in white adipocytes by peroxisome proliferator-activated receptor gamma agonists. *Mol. Cell. Biol.* **29**, 4714-4728.

Yamasaki, H., Sada, A., Iwata, T., Niwa, T., Tomizawa, M., Xanthopoulos, K. G., Koike, T. and Shiojiri, N. (2006). Suppression of C/EBPalpha expression in periportal hepatoblasts may stimulate biliary cell differentiation through increased Hnf6 and Hnf1b expression. *Development* **133**, 4233-4243.

Yoshida, Y., Hughes, D. E., Rausa, F. M., III, Kim, I. M., Tan, Y., Darlington, G. J. and Costa, R. H. (2006). C/EBPalpha and HNF6 protein complex formation stimulates HNF6-dependent transcription by CBP coactivator recruitment in HepG2 cells. *Hepatology* **43**, 276-286.

Cell Stem Cell
Short Article

Modeling Alzheimer's Disease with iPSCs Reveals Stress Phenotypes Associated with Intracellular Aβ and Differential Drug Responsiveness

Takayuki Kondo,[1,2,7] Masashi Asai,[7,9,10] Kayoko Tsukita,[1,7] Yumiko Kutoku,[11] Yutaka Ohsawa,[11] Yoshihide Sunada,[11] Keiko Imamura,[1] Naohiro Egawa,[1] Naoki Yahata,[1,7] Keisuke Okita,[1] Kazutoshi Takahashi,[1] Isao Asaka,[1] Takashi Aoi,[1] Akira Watanabe,[1] Kaori Watanabe,[7,10] Chie Kadoya,[7,10] Rie Nakano,[7,10] Dai Watanabe,[3] Kei Maruyama,[9] Osamu Hori,[12] Satoshi Hibino,[13] Tominari Choshi,[13] Tatsutoshi Nakahata,[1] Hiroyuki Hioki,[4] Takeshi Kaneko,[4] Motoko Naitoh,[5] Katsuhiro Yoshikawa,[5] Satoko Yamawaki,[5] Shigehiko Suzuki,[5] Ryuji Hata,[14] Shu-ichi Ueno,[15] Tsuneyoshi Seki,[16] Kazuhiro Kobayashi,[16] Tatsushi Toda,[16] Kazuma Murakami,[6] Kazuhiro Irie,[6] William L. Klein,[17] Hiroshi Mori,[18] Takashi Asada,[19] Ryosuke Takahashi,[2] Nobuhisa Iwata,[7,10,*] Shinya Yamanaka,[1,8] and Haruhisa Inoue[1,7,8,*]
[1]Center for iPS Cell Research and Application (CiRA)
[2]Department of Neurology, Graduate School of Medicine
[3]Department of Biological Sciences, Graduate School of Medicine and Department of Molecular and Systems Biology, Graduate School of Biostudies
[4]Department of Morphological Brain Science, Graduate School of Medicine
[5]Department of Plastic and Reconstructive Surgery, Graduate School of Medicine
[6]Organic Chemistry in Life Science, Division of Food Science and Biotechnology, Graduate School of Agriculture
Kyoto University, Kyoto 606-8507, Japan
[7]Core Research for Evolutional Science and Technology (CREST)
[8]Yamanaka iPS Cell Special Project
Japan Science and Technology Agency (JST), Saitama 332-0012, Japan
[9]Department of Pharmacology, Faculty of Medicine, Saitama Medical University, Saitama 350-0495, Japan
[10]Laboratory of Molecular Biology and Biotechnology, Department of Molecular Medicinal Sciences, Graduate School of Biomedical Sciences, Nagasaki University, Nagasaki 852-8521, Japan
[11]Department of Neurology, Kawasaki Medical School, Okayama 701-0192, Japan
[12]Department of Neuroanatomy (Biotargeting), Kanazawa University Graduate School of Medical Sciences, Ishikawa 920-8640, Japan
[13]Faculty of Pharmacy and Pharmaceutical Sciences, Fukuyama University, Hiroshima 729–0292, Japan
[14]Department of Functional Histology
[15]Department of Psychiatry
Ehime University Graduate School of Medicine, Ehime 791-0295, Japan
[16]Division of Neurology/Molecular Brain Science, Kobe University Graduate School of Medicine, Kobe, Hyogo 650-0017, Japan
[17]Department of Neurobiology, Northwestern University, Evanston, IL 60208, USA
[18]Department of Neuroscience, Graduate School of Medicine, Osaka City University, Osaka 545-8585, Japan
[19]Department of Neuropsychiatry, Institute of Clinical Medicine, University of Tsukuba, Ibaraki 305-8577, Japan
*Correspondence: haruhisa@cira.kyoto-u.ac.jp (H.I.), iwata-n@nagasaki-u.ac.jp (N.I.)
http://dx.doi.org/10.1016/j.stem.2013.01.009

SUMMARY

Oligomeric forms of amyloid-β peptide (Aβ) are thought to play a pivotal role in the pathogenesis of Alzheimer's disease (AD), but the mechanism involved is still unclear. Here, we generated induced pluripotent stem cells (iPSCs) from familial and sporadic AD patients and differentiated them into neural cells. Aβ oligomers accumulated in iPSC-derived neurons and astrocytes in cells from patients with a familial amyloid precursor protein (APP)-E693Δ mutation and sporadic AD, leading to endoplasmic reticulum (ER) and oxidative stress. The accumulated Aβ oligomers were not proteolytically resistant, and docosahexaenoic acid (DHA) treatment alleviated the stress responses in the AD neural cells. Differential manifestation of ER stress and DHA responsiveness may help explain variable clinical results obtained with the use of DHA treatment and suggests that DHA may in fact be effective for a subset of patients. It also illustrates how patient-specific iPSCs can be useful for analyzing AD pathogenesis and evaluating drugs.

INTRODUCTION

Alzheimer's disease (AD) is the most prevalent neurodegenerative disorder. One of the pathological features of AD is the oligomerization and aggregation and accumulation of amyloid-β peptide (Aβ), forming amyloid plaques in the brain. Cognitive impairment observed in clinical AD is inversely well correlated with the amount of Aβ oligomers in the soluble fraction rather than the amount of Aβ fibrils (amyloid plaques) constituting the oligomers (Haass and Selkoe, 2007; Krafft and Klein, 2010). Increasing evidence has shown that Aβ oligomers extracted from AD model mice or made from synthetic peptides cause

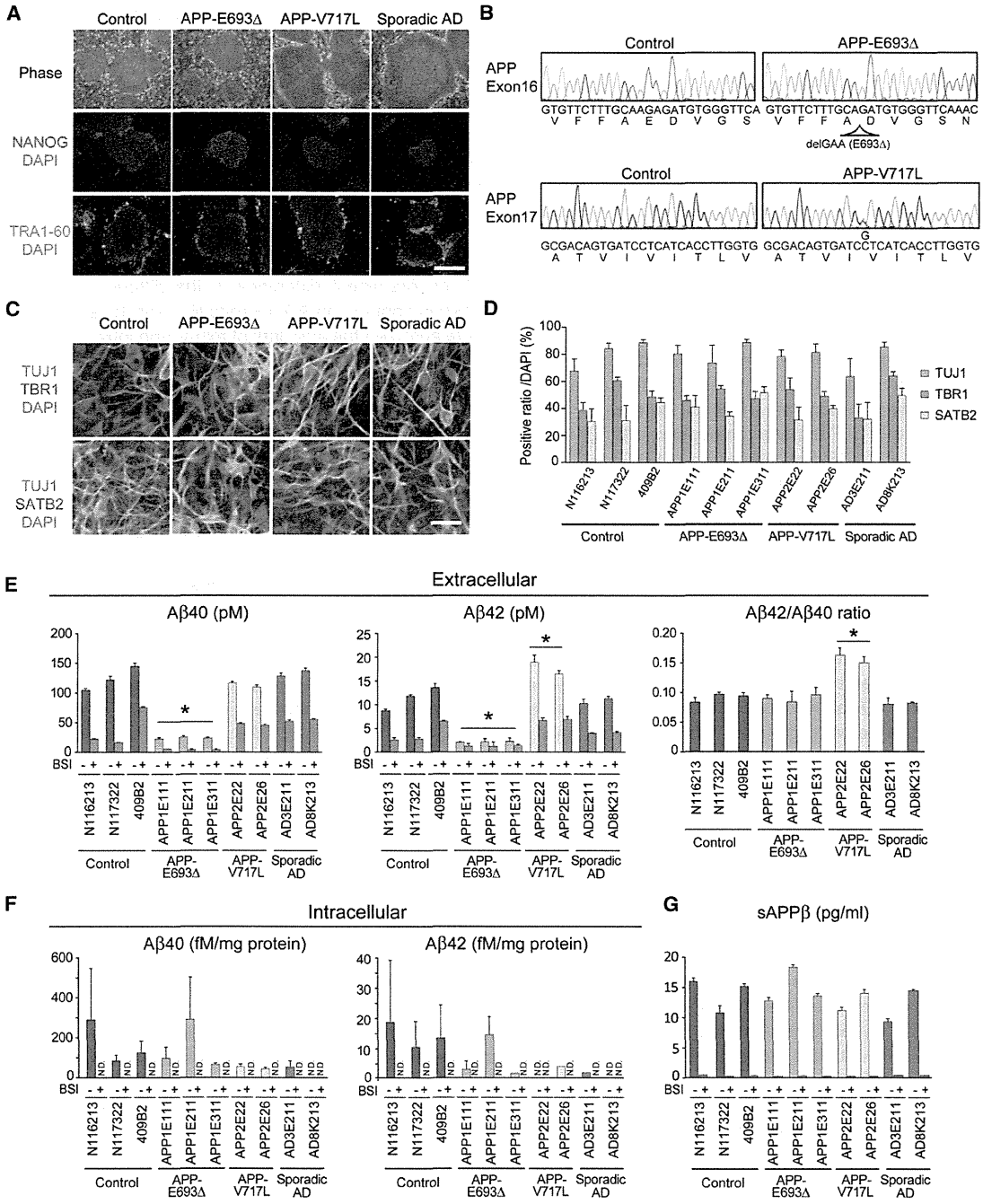

Figure 1. Establishment of Control and AD Patient-Specific iPSCs, and Derivation of Cortical Neurons Producing Aβs from iPSCs

(A) Established iPSCs from both controls and AD patients showed embryonic stem cell-like morphology (Phase) and expressed pluripotent stem cell markers NANOG (red) and TRA1-60 (green). The scale bar represents 200 μm.

(B) Genomic DNA sequences showed the presence of the homozygous genotype for E693 deletion and the heterozygous genotype for V717L mutation on the *APP* gene only in AD iPSCs.

(C) Estimation of neuronal differentiation from control and AD-iPSCs. After 2 months of differentiation, neurons were immunostained with antibodies against the neuronal marker TUJ1 and the cortical neuron markers TBR1 and SATB2. The scale bar represents 30 μm.

(D) Proportions of TUJ1-, TBR1-, and SATB2-positive cells in control and AD-iPSCs. Data represent mean ± SD (n = 3 per clone).

(E) Aβ40 and Aβ42 secreted from iPSC-derived neural cells into the medium (extracellular Aβ) were measured at 48 hr after the last medium change. Data represent mean ± SD (n = 3 per clone). Levels of Aβ40 and Aβ42 in AD(APP-E693Δ) without β-secretase inhibitor IV (BSI, 1 μM) were significantly lower than those of the others (*, $p < 0.006$), and the level of Aβ42 and the ratio of Aβ42/Aβ40 in AD(APP-V717L) without BSI were significantly higher than those of the others

(legend continued on next page)

neurotoxicity and cognitive impairments in vitro and in vivo (Walsh et al., 2002; Gong et al., 2003; Lesné et al., 2006), and this was also true in humans (Kuo et al., 1996; Shankar et al., 2008; Noguchi et al., 2009). Therefore, the formation and accumulation of Aβ oligomers has been presumed to play a central role in the pathogenesis and clinical symptoms of AD. Aβs are composed of 38–43 amino acid residues and are generated from the amyloid precursor protein (APP) by β- and γ-secretase-mediated sequential cleavages. A number of mutations linked to familial AD in the *APP* gene have been identified. Recently, an atypical early-onset familial AD, caused by an E693Δ mutation of an APP-producing variant Aβ lacking 22nd Glu was discovered in Japan (Tomiyama et al., 2008). This APP-E693Δ mutation presents rare, autosomal-recessive mutations of the *APP* gene related to familial AD. Patients with the mutation show overt early-onset symptoms of AD but lack Aβ deposition, according to positron emission tomography (PET) scan analysis with a [^{11}C] Pittsburgh compound-B (PIB) radioprobe (Tomiyama et al., 2008; Shimada et al., 2011). The 22nd Glu within the Aβ sequence has a destabilizing effect on the formation of oligomeric structures because of the electrostatic repulsion between the adjacent side chain of 22nd Glu (Kassler et al., 2010), and the deletion of the amino acid residue leads to the ready formation of Aβ oligomers in vitro (Nishitsuji et al., 2009). APP-E693Δ transgenic mice show AD-like pathology, including intracellular oligomer accumulation, but lack extracellular amyloid plaque formation (Tomiyama et al., 2010). However, it remains unclear whether Aβ oligomers are accumulated in familial and sporadic AD patient neural cells and how intracellular Aβ oligomers play a pathological role. The compound and/or drugs that might rescue the Aβ oligomer-induced pathological phenotypes are also unclear. Recent developments in induced pluripotent stem cell (iPSC) technology have facilitated the investigation of phenotypes of patient neural cells in vitro and have helped to overcome the lack of success in modeling sporadic AD.

Here, we report the derivation and neuronal and astroglial differentiation of iPSCs from a familial AD patient with an APP-E693Δ mutation, a familial case with another APP mutation, as well as other sporadic cases. Using patient neurons and astrocytes, we addressed the accumulation and possible pathological roles of intracellular Aβ oligomers in familial and sporadic AD. We found that Aβ oligomers were not proteolytically resistant and that docosahexaenoic acid (DHA) treatment attenuated cellular phenotypes of AD neural cells with intracellular Aβ oligomers in both familial and sporadic AD patients.

RESULTS

iPSC Generation and Cortical-Neuronal Differentiation

Dermal fibroblasts were reprogrammed by episomal vectors (Okita et al., 2011). Control iPSC lines from three unrelated individuals, three and two familial AD iPSC lines from patients with E693Δ[AD(APP-E693Δ)] and V717L[AD(APP-V717L)] APP mutations, respectively, and two sporadic iPSC lines (AD3E211 and AD8K213) from two unrelated patients (Figure S1A available online) were generated (Figures 1A, 1B, and S1B–S1H). To characterize cortical neurons derived from the iPSC lines, we established differentiation methods for cortical neurons by modifying previous procedures (Morizane et al., 2011) (Figure S1I). The differentiated cells expressed the cortical neuron subtype markers SATB2 and TBR1 (Figure 1C), and the differentiated neurons were functionally active (Figures S1J and S1K). There was no prominent difference in the differentiation propensity between control and AD neurons (Figures 1D and S1L).

We analyzed the amounts of extra- and intracellular Aβ40 and Aβ42 (Figures 1E and 1F). As expected, both Aβ species were strongly decreased in all cloned AD(APP-E693Δ) neural cells in comparison to those in control neural cells. In familial AD(APP-V717L) neural cells, an increase in the extracellular Aβ42 level and a corresponding decrease in the intracellular Aβ42 level were observed, and the Aβ42/Aβ40 ratio in the culture medium was increased up to 1.5-fold, suggesting that the abnormality of APP metabolism in AD is dependent on the mutation sites in *APP*. Extracellular Aβ levels in sporadic AD neural cells were not changed in comparison to those in control neural cells, but intracellular Aβ in sporadic AD8K213 neural cells apparently decreased (that is, below the detection limit). APP expression levels in the AD(APP-E693Δ) neural cells were lower than in the others, but the levels of α- and β-secretase-mediated APP processing remained unaltered in all neural cells (Figures 1G, S1M, and S1N). Soluble APPβ production was strongly inhibited by treatment with β-secretase inhibitor IV (BSI) (Figure 1G). Aβ levels in the original fibroblasts and iPSC-derived astrocytes, in which APP expression levels were relatively higher than those in neural cells (data not shown), were lower than those of the corresponding neural cells (Figures S1O and S1P).

Intracellular Accumulation of Aβ Oligomers in AD(APP-E693Δ) and in One of the Sporadic AD Neural Cells

Using an immunocytochemical method with the Aβ-oligomer-specific antibody NU1 (Lambert et al., 2007), we investigated whether AD(APP-E693Δ) neural cells harbor Aβ oligomers or not. We found that Aβ oligomers were accumulated as puncta in the neurons of AD(APP-E693Δ) and in one of the sporadic AD cases (Figure 2A). The area of Aβ-oligomer-positive puncta was significantly increased in AD(APP-E693Δ) neuronal cells relative to control neuronal cells (Figure 2B). Dot blot analysis using cell lysates revealed that Aβ oligomers were markedly elevated in the AD(APP-E693Δ) and sporadic AD8K213 neural cells (Figures 2C and 2D), whereas Aβ oligomers were not detected in the culture medium (data not shown). Another antibody against Aβ, 11A1, which detects low-molecular-weight oligomers rather than the Aβ monomer (Murakami et al., 2010), showed results similar to those observed with NU1 (Figures

(*, $p < 0.001$). There are significant differences between dimethyl sulfoxide (DMSO)-control and BSI treatment in each case (*, $p < 0.001$) except that of AD(APP-E693Δ) for Aβ42.
(F) Aβ40 and Aβ42 in cell lysates (intracellular Aβ). N.D., not detected. Data represent mean ± SD (n = 3 per clone).
(G) The amount of soluble APPβ was not altered in control and AD. Data represent mean ± SD (n = 3 per clone).
See also Figure S1.

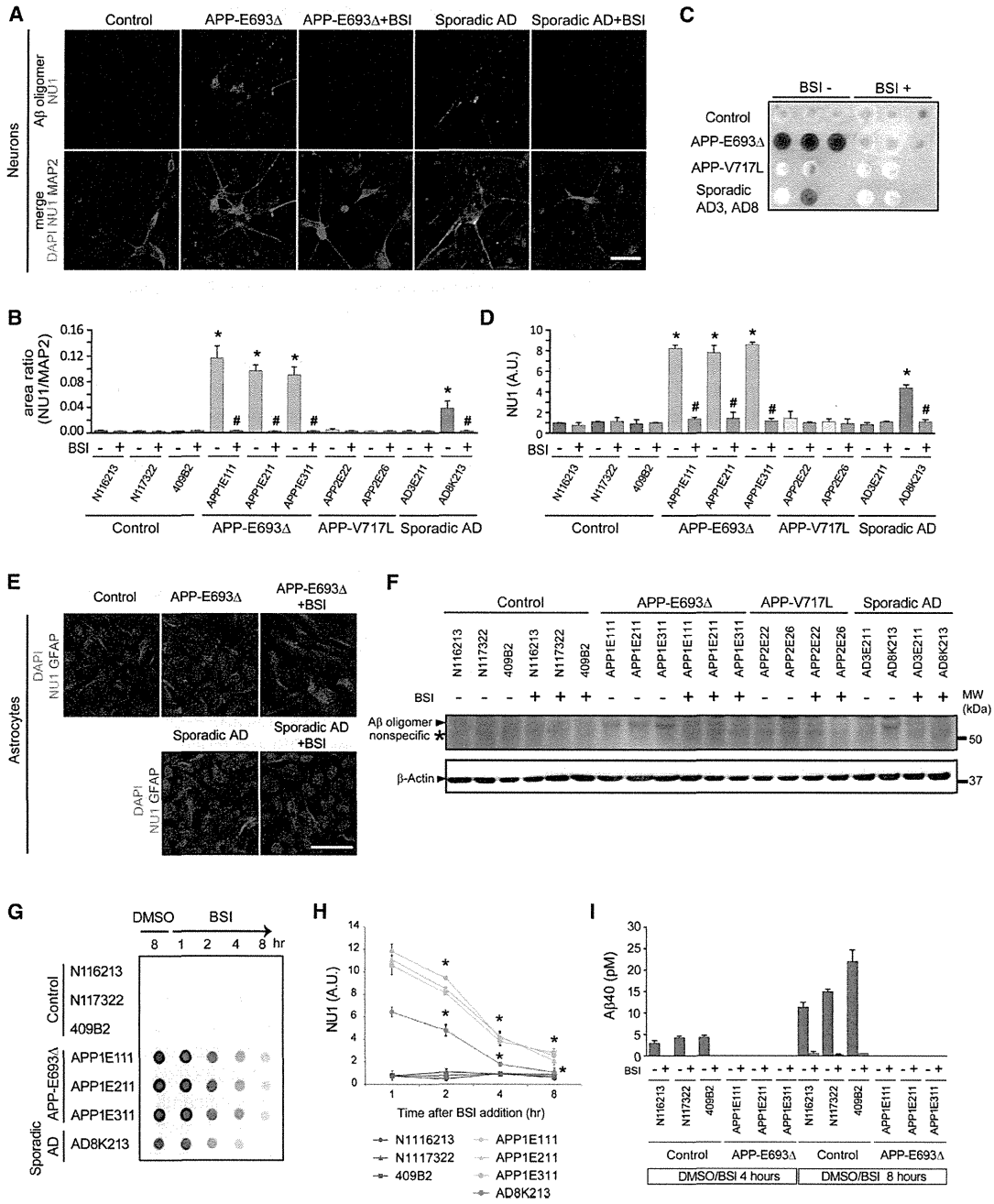

Figure 2. Familial AD(APP-E693Δ) and Sporadic AD iPSC-Derived Neurons Have Intracellular Aβ Oligomers

(A) Intracellular Aβ oligomer accumulation in iPSC-derived neurons (red, MAP2-positive cells) was detected by the Aβ-oligomer-specific monoclonal antibody NU1 (green) with a punctate pattern. Aβ oligomer accumulation was massive in AD(APP-E693Δ) and sporadic AD(AD8K213) neurons but only faint in control neurons. Treatment with 1 μM BSI decreased Aβ oligomer accumulation. DAPI, nuclear staining (blue). The scale bar represents 30 μm.

(B) Quantification of Aβ oligomer accumulation in (A); the ratio of the NU1-positive area in the MAP2-positive area was analyzed. Data represent mean ± SD (n = 3 per clone). Aβ oligomer levels in the AD(APP-E693Δ) and sporadic AD(AD8K213) neural cells without BSI were significantly different from those of other neural cells (*, $p < 0.005$) and from corresponding neural cells with BSI (#, $p < 0.005$).

(C) Dot blot analysis with the use of NU1 antibody. Control (N116213, N117322, 409B2), APP-E693Δ(APP1E111, APP1E211, APP1E211), APP-V717L (APP2E22, APP2E26), and sporadic AD (AD3E211, AD8K213) neural cells were dotted from the left. Blank is RIPA buffer only.

(D) Signals of blot in (C) were quantified. Data represent mean ± SD (n = 3 per clone). Aβ oligomer levels in AD(APP-E693Δ) and sporadic AD(AD8K213) neurons without BSI were significantly different from those of other neurons (*, $p < 0.001$) and from corresponding neurons treated with 1 μM BSI (#, $p < 0.001$).

(E) Aβ oligomer accumulation in AD astrocytes. The scale bar represents 30 μm.

(legend continued on next page)

S2A–S2D). However, Aβ oligomers were not detected in cell lysates from the fibroblasts that generate iPSC lines (Figure S2E). To confirm whether Aβ oligomers were derived from mutant APP(E693Δ), we transduced a lentiviral vector driven by an EF1α promoter to overexpress wild or mutant APP(E693Δ) in control iPSC-derived neural cells and found that Aβ oligomers emerged inside control neural cells overexpressing mutant APP(E693Δ) (Figure S2F).

To investigate the intracellular accumulation of Aβ oligomers in astrocytes derived from control and AD iPSCs, we established an astrocyte-enrichment culture by modifying the method previously reported (Krencik et al., 2011) (Figures S2G–S2J). Dot blot analysis using Aβ oligomer antibodies revealed that the astrocytes of AD(APP-E693Δ) and one of the sporadic AD iPSCs accumulated Aβ oligomers intracellularly (Figures 2E, S2K, and S2L), which was compatible with the results of neurons. On the other hand, we detected no difference in the uptake of extracellular glutamate between control and AD astrocytes (Figure S2M).

Aβ oligomers were also detected as a protein band with a molecular mass of 50~60 kDa by western blot analysis (Figures 2F and S2N). The accumulation of Aβ oligomers was inhibited by treatment with BSI (Figures 2A–2G, S2A–S2D, and S2N). To clarify whether the E693Δ mutation results in accelerated Aβ oligomerization and/or in a proteolytically resistant and stable form of Aβ oligomers, we analyzed the levels of Aβ oligomers over a course of time after BSI treatment. Intracellular Aβ oligomers started to disappear from 2 hr after the treatment with BSI, almost reaching the control level by 8 hr (Figures 2G and 2H). Secretion of Aβ40 from control neural cells was already inhibited at 2 hr after BSI treatment, but the secretion from AD neural cells was under the detection limit in both the presence and absence of BSI (Figure 2I).

Cellular Stress Responses Caused By Intracellular Aβ Oligomers in AD iPSC-Derived Neural Cells

Extracellular Aβ deposition in patient brains carrying APP with an E693Δ mutation is predicted to be extremely low, as amyloid PET imaging with a [^{11}C] PIB probe revealed a far lower signal in the patients than those observed in sporadic AD brains (Tomiyama et al., 2008). Given that processing by β- and γ-secretases largely proceeds within vesicular endosomal compartments, it was possible that Aβ oligomers were associated with specific organelles. We characterized the Aβ oligomer-positive punctate structures in AD(APP-E693Δ) neural cells and astrocytes by coimmunostaining with antibodies for markers of vesicular compartments and subcellular organelles. Subpopulations of Aβ oligomer-positive puncta in the AD neurons showed positive immunostaining for an endoplasmic reticulum (ER) marker, binding immunoglobulin protein (BiP); an early endosomal marker, early endosome-associated antigen-1 (EEA1); and a lysosomal marker, lysosomal-associated marker protein 2 (LAMP2) (data not shown).

To uncover molecules that might be implicated in the dysfunction of AD(APP-E693Δ) neural cells, we analyzed gene expression profiles of control and AD neural cells (Figure 3A and Table S1). Gene ontology analysis revealed that oxidative-stress-related categories, including peroxiredoxin, oxidoreductase, and peroxidase activities, were upregulated in the AD, whereas glycosylation-related categories were downregulated (Figures 3B and 3C and Table S1), suggesting that ER and Golgi function might be perturbed in AD neural cells. Western blot analysis clarified that the amounts of both BiP and cleaved caspase-4 were elevated in the neurons and astrocytes of the AD(APP-E693Δ) case, and that of BiP in one of the sporadic AD cases, AD8K213, but not in fibroblasts (Figures 3D–3F and S3A–S3F). We also found that BSI treatment not only prevented the increase in Aβ oligomer-positive puncta area per cell in the context of AD(APP-E693Δ) lines but also decreased the amount of BiP and cleaved caspase-4 (Figures 3D–3F). *PRDX4*-coding antioxidant protein peroxiredoxin-4 was the most highly upregulated gene (Figure 3C). Western blot analysis confirmed that the amount of peroxiredoxin-4 was increased up to approximately 5- to 7-fold in lysates from AD(APP-E693Δ) and in one of the sporadic AD cases, AD8K213 neural cells, but not in fibroblasts, and was decreased by the BSI treatment (Figures 3D, 3G, S3A, S3D, S3G, and S3H), indicating that the antioxidant stress response was provoked by Aβ oligomer formation in AD(APP-E693Δ) and sporadic AD8K213. To identify pathogenic species evoking oxidative stress in AD(APP-E693Δ), we visualized reactive oxygen species (ROS) and found that ROS was increased in both neurons and astrocytes in AD(APP-E693Δ) and AD8K213 (Figures 3H–3J and S3I –S3L). This increase was counteracted by the BSI treatment. These results indicated that intracellular Aβ oligomers provoked both ER and oxidative stress, and the increase in ROS most likely occurred via a vicious cycle between ER and oxidative stress (Malhotra and Kaufman, 2007).

Alleviation of Intracellular Aβ Oligomer-Induced Cellular Stress by DHA

We evaluated BSI and three additional drugs that had been reported to improve ER stress or to inhibit ROS generation: (1) DHA (Begum et al., 2012), (2) dibenzoylmethane (DBM14-26) (Takano et al., 2007), and (3) NSC23766 (Lee et al., 2002) (Figures 4 and S4). DHA treatment significantly decreased the protein level of BiP, cleaved caspase-4, and peroxiredoxin-4 in AD (APP-E693Δ) neural cells (Figures 4A, 4B, S4A, and S4B), and BiP and peroxiredoxin-4 in sporadic AD8K213 (Figures S4C and S4D). Furthermore, DHA treatment also decreased the generation of ROS in AD(APP-E693Δ) neural cells (Figures 4C and 4D), whereas the amount of Aβ oligomers in cell lysates

(F) Western blot analysis of control and AD neural cells in the presence or absence of BSI. BSI treatment (1 μM) disappeared 6E10-positive ≈55 kDa protein bands in cell lysates of AD(APP-E693Δ) and sporadic AD(AD8K213) neural cells.

(G) Disappearance of Aβ oligomers after BSI treatment was analyzed by dot blot analysis with the use of the NU1 antibody. Intracellular Aβ oligomers started to disappear 2 hr after BSI treatment.

(H) Signals of blots in (G) were quantified. Data represent mean ± SD (n = 3 per clone). BSI treatment (1 μM) decreased intracellular Aβ in AD neural cells and was reduced to 16~23% of vehicle control by 8 hr. Post hoc analysis revealed that the amounts of Aβ oligomers at 2 hr after BSI treatment were significantly decreased in comparison to those of DMSO control oligomers (*, $p < 0.005$).

(I) Changes in extracellular Aβ40 levels were analyzed in the experimental condition of (G). Data represent mean ± SD (n = 3 per clone).

See also Figure S2.

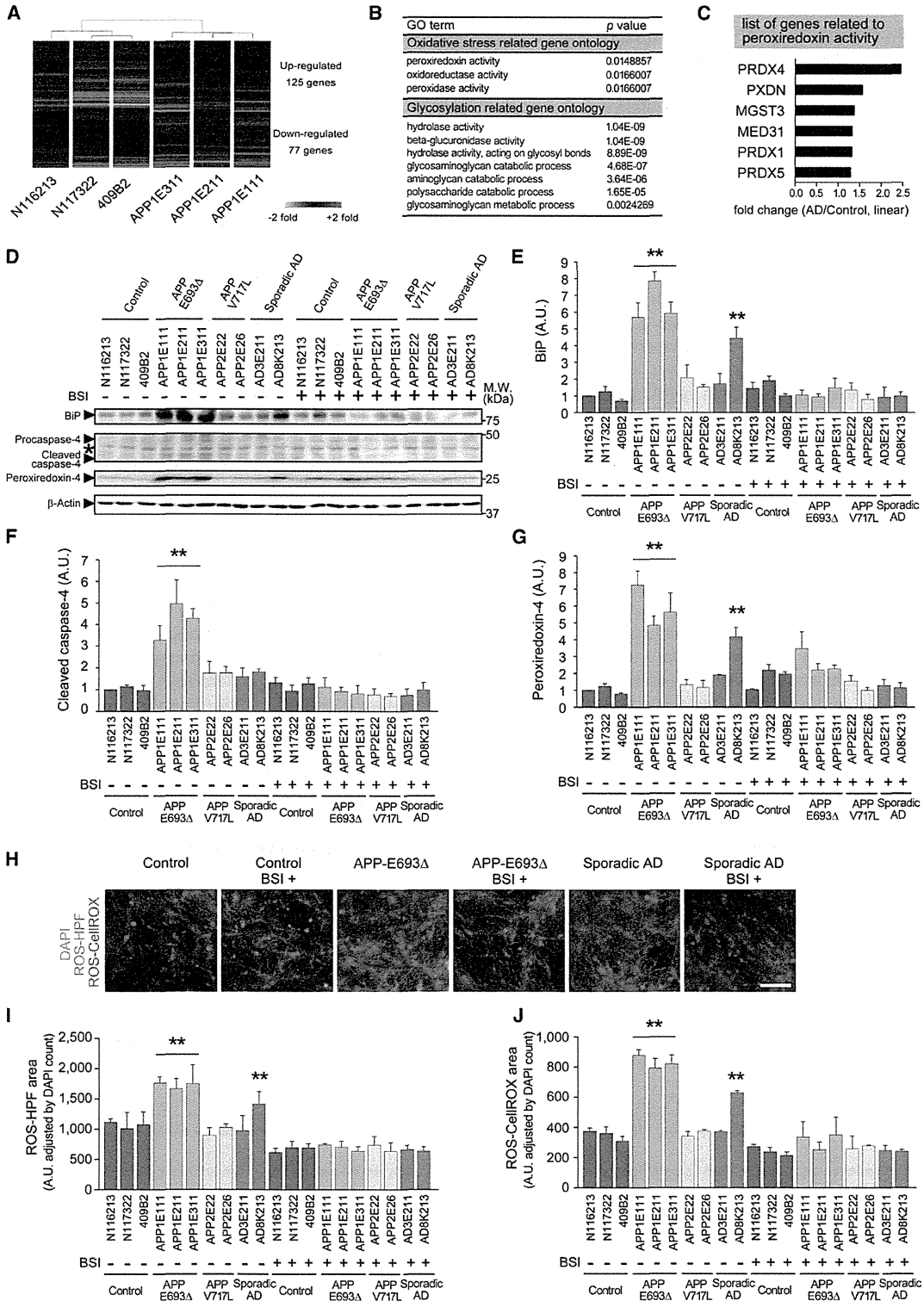

Figure 3. Cellular Stress Responses Caused by Intracellular Aβ Oligomers in Familial AD(APP-E693Δ) and Sporadic AD(AD8K213) iPSC-Derived Neural Cells

(A) Hierarchical clustering analysis of differentiated neuronal cells and a heatmap of significantly up- and downregulated genes in AD neural cells. The statistically significant cutoff p value is < 0.05.

(legend continued on next page)

was not altered (Figures S4E–S4G). In contrast, the high concentration of DHA, DBM14-26, or NSC23766 treatment increased the protein level of BiP (Figure S4B). Finally, to confirm the protective effects of DHA in short-term screening, we analyzed the effect on the survival of AD(APP-E693Δ) neural cells. Neuronal cells were labeled with a lentiviral vector expressing synapsin I-promoter-driven EGFP and cultivated in the medium depleted of neurotrophic factors and neural culture supplements mix. The real-time survival rate of AD(APP-E693Δ) neurons was lower than that of normal control neurons; however, DHA treatment for 16 days partially rescued AD(APP-E693Δ) cell viability (Figures 4E–4G). The real-time survival rate of sporadic AD(AD3E211, AD8K213) neurons for 16 days was unchanged (Figures 4E and 4F and Table S2). We confirmed these results through a lactate dehydrogenase (LDH) assay (Figure 4G). The AD(APP-E693Δ) neurons were also vulnerable to oxidative stress by hydrogen peroxide treatment (Figure S4H). Extracellular Aβ levels were not altered in the assay (Figure 4H).

DISCUSSION

The present study shows that neural cells derived from a patient carrying the pathogenic APP-E693Δ mutation and a sporadic AD patient produce intracellular Aβ oligomers, and the use of these neural cells provided an experimental system for addressing whether such oligomers would cause cellular stress and the killing of neurons and how such intracellular Aβ oligomers might contribute to the disease pathogenesis, despite only one patient carrying the E693Δ mutation being available. Our findings also suggest that the possible heterogeneity of familial and sporadic AD stems from phenotypic differences of intracellular Aβ oligomers and suggests the possibility that DHA, a drug that failed in some clinical trials of AD treatment, might be effective in a portion of AD patients.

We demonstrated that Aβ oligomers were formed and accumulated inside AD(APP-E693Δ) and sporadic AD(AD8K213) neurons by immunostaining (Figures 2A and 2B), dot blot analysis (Figures 2C and 2D), and western blot analysis (Figures 2F and S2N). In addition, intracellular accumulation of Aβ oligomers, which has been supposed to be proteolytically resistant, disappeared after treatment with BSI in both AD neurons (Figures 2G and 2H), indicating that AD(APP-E693Δ) and sporadic AD(AD8K213) neurons still seemed to retain a degrading activity toward Aβ oligomers in which proteasomes, autophagosomes, and/or lysosomes may be involved and, thereby, that the pathological property of Aβ oligomers in a part of AD might be completely abrogated. The sporadic AD(AD8K213) neurons may retain a specific cellular environment that permits the formation of Aβ oligomers. Additional studies aimed at identifying the factors causing such an environment are needed.

We observed that the accumulation of Aβ oligomers induced ER and oxidative stress both in AD(APP-E693Δ) and in sporadic AD(AD8K213) neurons, although caspase-4 activation appeared not to accompany sporadic AD, probably because of the lesser extent of ER stress in comparison to AD(APP-E693Δ). Previously, Nishitsuji et al. (2009) reported that accumulated Aβ oligomers in ER provoke ER stress. This result suggests that oligomers represent a self-aggregating state of Aβ. During this process, Aβ generates ROS, which is supported by the fact that Aβ coordinates the metal ions zinc, iron, and copper, which induce the oligomerization of Aβ. Iron and copper then cause the generation of toxic ROS and calcium dysregulation (Barnham et al., 2004), leading to membrane lipid peroxidation and the impairment of the function of a range of membrane-associated proteins (Hensley et al., 1994; Butterfield, 2003), antioxidant factors being thought to protect ER-stress-induced cellular toxicities (Malhotra and Kaufman, 2007).

We found that intracellular Aβ oligomers were accumulated not only in a case of familial AD with APP-E693Δ mutation but also in a sporadic AD case, although only three clones derived from one familial AD patient carrying an APP-E693Δ mutation and two clones from two sporadic AD patients were analyzed in this study because of the limited number of patients. In contrast, in familial AD with the APP-V717L mutation, of which only one case was available, intracellular Aβ oligomers were not detected, but the extracellular Aβ42/Aβ40 ratio, which is increased in mutant presenilin-mediated familial AD, as reported previously (Yagi et al., 2011), was increased, lending support to the notion that AD could be classified into two categories: extracellular Aβ type and intracellular Aβ type. Although it has been supposed that environmental factors and/or the aging process contribute to neurodegenerative diseases, our findings support the idea that a genetic factor might play a role in a part of sporadic AD, a finding that is compatible with a previous report (Israel et al., 2012). However, identifying the genetic factor would require a larger sample size. The sporadic AD case with intracellular Aβ oligomers might correspond to the case without extracellular Aβ40 elevation of Israel et al. (2012). Analysis of neurons

(B) The gene ontology (GO) term list, calculated from the significantly altered gene expression patterns in the microarray analysis of AD versus control neural cells.

(C) Altered expression levels of genes related to peroxidation activity detected by GO analysis. All values were significantly different from that of the control ($p < 0.05$).

(D–G) Western blot analysis of ER stress markers (BiP and casapase-4), peroxiredoxin-4, and a reference protein (β-actin) in the presence or absence of BSI. (E–G) Densitometric analysis of (D) are shown. Measured values of proteins were normalized by β-actin. Data represent mean ± SD (n = 3 per clone). Levels of BiP (E), cleaved caspase-4 (F), and peroxiredoxin-4 (G) in AD(APP-E693Δ) and sporadic AD(AD8K213) neural cells without BSI were significantly different from those of the other neural cells (**, $p < 0.005$).

(H) Typical images of reactive oxygen species (ROS) staining, detected by HPF or CellROX, in control and AD neural cells with or without BSI treatment. Scale bars represent 30 μm.

(I and J) Quantitative data of (H), ROS-HPF (I), and ROS-CellROX (J). Each value was shown as a ratio of the HPF-stained or CellROX area (average of random 25 fields per sample) adjusted with DAPI counts. Data represent mean ± SD (n = 3 per clone). ROS-generation levels in AD(APP-E693Δ) and sporadic AD(AD8K213) neural cells were significantly different from those of the others (**, $p < 0.001$). Data represent mean ± SD (n = 3 per clone).

See also Figure S3 and Table S1.

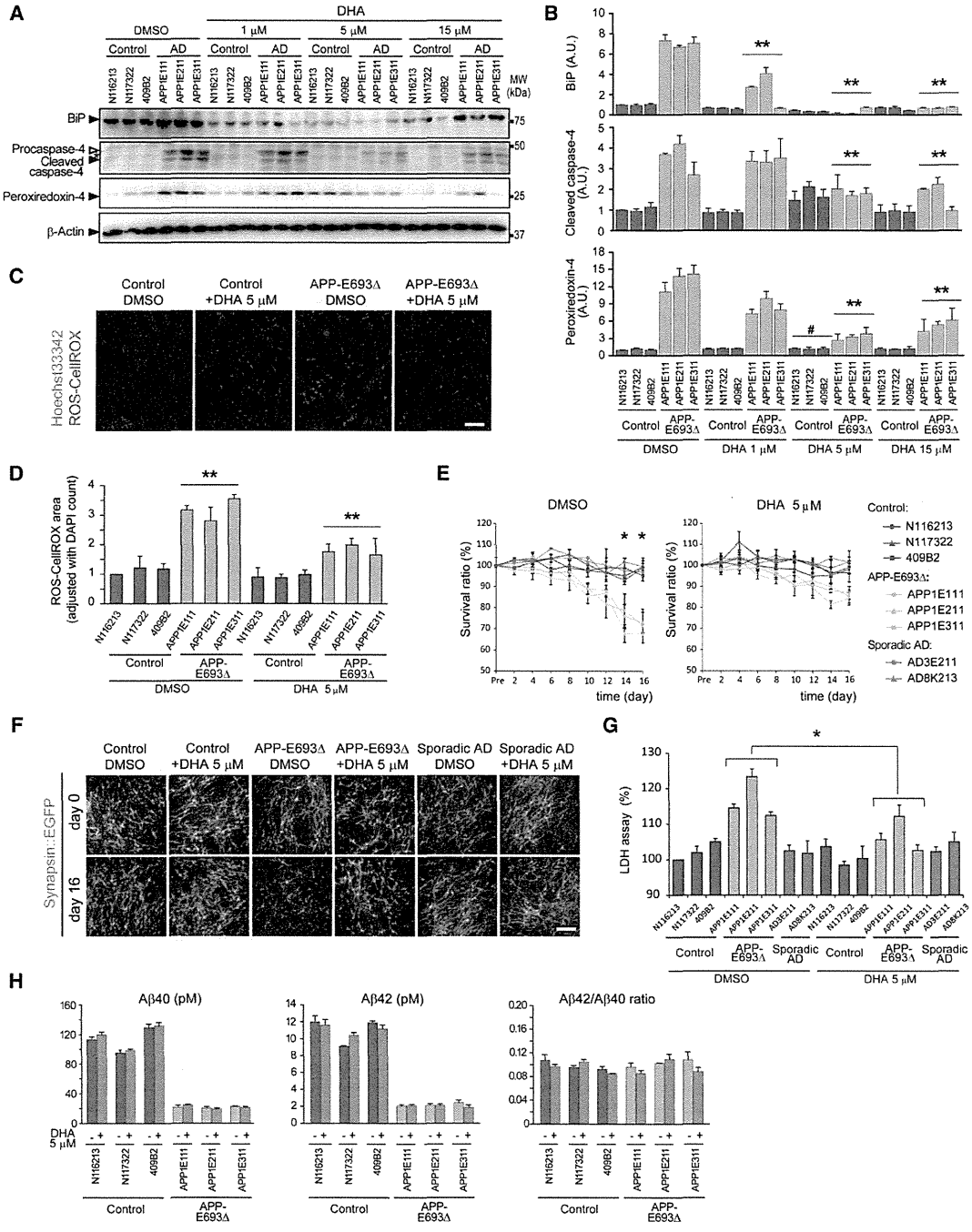

Figure 4. DHA-Alleviated Cellular Stress Caused By Intracellular Aβ Oligomers

(A) Control and AD(APP-E693Δ) neural cells at day 72 were treated with DHA for 48 hr. Then, cells were lysed and subjected to immunoblot analysis (1 μM, 5 μM, and 15 μM of docosahexaenoic acid [DHA]).

(B) Densitometric analysis of (A) is shown. Measured values were normalized by that of β-actin. Data represent mean ± SD (n = 3 per clone). Two-way analysis of variance (ANOVA) showed significant main effects of DHA treatment (BIP, $F_{[3,64]} = 136.712$, $p < 0.001$; cleaved caspase-4, $F_{[3,64]} = 50.855$, $p < 0.001$) with a significant interaction between APP mutation and DHA treatment (BIP, $F_{[3,64]} = 99.658$, $p < 0.001$; cleaved caspase-4, $F_{[3,64]} = 53.005$, $p < 0.001$). Post hoc analysis revealed significant differences between DMSO (control) and DHA treatment (1, 5, and 15 μM) in AD(APP-E693Δ) neural cells (**, $p < 0.001$). Two-way ANOVA for peroxiredoxin-4 showed significant main effects of DHA treatment ($F_{[3,64]} = 16.995$; $p < 0.001$) with a significant interaction between APP mutation and DHA treatment ($F_{[3,64]} = 32.093$; $p < 0.001$). Post hoc analysis revealed significant differences between DMSO-control and DHA treatment (5 and 15 μM) in AD(APP-E693Δ) neural cells (**, $p < 0.001$). In control neural cells, the 5 μM DHA group was significantly different from the other groups (#, $p < 0.005$).

(C) Typical images of ROS-CellROX and Hoechst33342 signals after treatment with vehicle or 5 μM DHA. The scale bar represents 50 μm.

(legend continued on next page)

and astrocytes, as we performed here, from larger numbers of patients might result in the classification of sporadic AD.

To date, the clinical effectiveness of DHA treatment is still controversial (Freund-Levi et al., 2006; Quinn et al., 2010). It is of particular interest that one of two sporadic AD neurons accumulated intracellular Aβ oligomers and showed cellular phenotypes that could respond to DHA but the other did not, and this result may explain why DHA treatment was effective for some AD patients, those with the intracellular Aβ oligomer-associated type of AD, although the timing (that is, the stage of disease development) for starting the treatment would be another critical factor. These results may suggest that patient-specific iPSCs provide a chance to re-evaluate the effect of a drug that failed in AD clinical trials, depending on the selection of the patient type. In the present study, the amount of Aβ oligomers in our culture was not affected by DHA, although it would be effective for reducing cellular stresses, and reducing the oligomerization of Aβ was also presumed to be a candidate mechanism of DHA treatment (Cole and Frautschy, 2006). These results indicate that therapy with DHA would alleviate symptoms. Furthermore, the data showing that BSI treatment leads to a reduction in ROS formation at a relatively similar level (Figure 2G) in both AD and control cells might indicate an Aβ oligomer-independent effect, in addition to an Aβ oligomer-dependent effect, of BSI.

In any event, patient-specific iPSCs would provide disease pathogenesis, irrespective of the disease being in a familial or sporadic form, as well as enable the evaluation of drug and patient classification of AD.

EXPERIMENTAL PROCEDURES

Derivation of Patient-Specific Fibroblasts

Control and AD-derived human dermal fibroblasts (HDFs) were generated from explants of 3 mm dermal biopsies. After 1–2 weeks, fibroblast outgrowths from the explants were passaged.

iPSC Generation

Human complementary DNAs for reprogramming factors were transduced in HDFs with episomal vectors (*SOX2, KLF4, OCT4, L-MYC, LIN28*, and small hairpin RNA for p53). Several days after transduction, fibroblasts were harvested and replated on an SNL feeder cell layer. On the following day, the medium was changed to a primate embryonic stem cell medium (ReproCELL, Japan) supplemented with 4 ng/ml basic FGF (Wako Pure Chemicals Industries, Japan). The medium was changed every other day. iPSC colonies were picked up 30 days after transduction.

Statistical Analysis

All data are shown as mean ± SD. For comparisons of the mean between two groups, statistical analysis was performed by applying Student's t tests after confirming equality between the variances of the groups. When the variances were unequal, Mann-Whitney U tests were performed (SigmaPlot 11.2.0, Systat Software, USA). Comparisons of the mean among three groups or more were performed by one-way, two-way, or three-way analysis of variance followed by a post hoc test with the use of Student-Newman-Keuls Method (SigmaPlot 11.2.0). p values < 0.05 were considered significant.

ACCESSION NUMBERS

The Gene Expression Omnibus accession numbers for microarray data reported in this paper are GSE43326 (gene-expression comparison between control and AD clones), GSE43382 (gene-expression change along with the astroglial differentiation), and GSE43328 (gene-expression comparison of generated iPSCs).

SUPPLEMENTAL INFORMATION

Supplemental Information contains Supplemental Experimental Procedures, four figures, and two tables and can be found with this article online at http://dx.doi.org/10.1016/j.stem.2013.01.009.

ACKNOWLEDGMENTS

We would like to express our sincere gratitude to all our coworkers and collaborators, Mari Ohnuki, Megumi Kumazaki, Mitsuyo Kawada, Fumihiko Adachi, Takako Enami, and Misato Funayama for technical assistance; Nobuya Inagaki and Norio Harada for technical advice; and Kazumi Murai for editing the manuscript. This research was funded in part by a grant from the Funding Program for World-Leading Innovative R&D on Science and Technology (FIRST Program) of the Japan Society for the Promotion of Science (JSPS) to S.Y., from the Alzheimer's Association (IIRG-09-132098) to H.M., from the JST Yamanaka iPS Cell Special Project to S.Y. and H.I., from CREST to H.I., H.M., N.I., and T.T., from a Grant-in-Aid from the Ministry of Health, Labour and Welfare of Japan to H.I., from a Grant-in-Aid for Scientific Research on Innovative Area "Foundation of Synapse and Neurocircuit Pathology" (22110007) from the Ministry of Education, Culture, Sports, Science and Technology of Japan to H.I. and N.I., and from the Japan Research Foundation for Clinical Pharmacology to H.I. H.I. conceived the project; T.K., N.I., M.A., and H.I. designed the experiments; T.K., N.I., M.A., K.W., C.K., R.N., N.E., N.Y. and K. Tsukita performed the experiments; T.K., N.I., M.A., and H.I. analyzed the data; K.O., I.A., K.M., T.N., K.I., W.L.K., O.H., S.H., and T.C. contributed

(D) Quantitative data of (C) is shown. Each value indicated the ratio of the CellROX-stained area (an average of random 25 fields per sample) adjusted with DAPI counts. Data represent mean ± SD (n = 3 per clone). Two-way ANOVA showed significant main effects of DHA treatment ($F_{[1,32]} = 43.140$; $p < 0.001$) with a significant interaction between the APP mutation and DHA treatment ($F_{[3,32]} = 23.410$; $p < 0.001$). The DHA group in AD(APP-E693Δ) neural cells was significantly different from the other groups (**, $p < 0.005$).

(E) Real-time survival rate of control and AD neural cells with and without DHA showing cell viability. The numbers of control and AD(APP-E693Δ) neurons with Synapsin I-promoter-driven EGFP were sequentially imaged (average of 25 random fields per sample) and counted to assess the survival ratio (n = 3 per clone). Data represent mean ± SD (n = 3 per clone). In the cell-survival ratio, three-way ANOVA showed significant main effects of the APP mutation ($F_{[1,256]} = 377.611$; $p < 0.001$), DHA treatment ($F_{[1,256]} = 36.117$; $p < 0.001$), and time ($F_{[7,256]} = 65.272$; $p < 0.001$), with significant interactions between the APP mutation and DHA treatment ($F_{[1,256]} = 18.315$; $p < 0.001$), between the APP mutation and time ($F_{[7,256]} = 20.023$; $p < 0.001$), between DHA treatment and time ($F_{[7,256]} = 4.534$; $p < 0.001$), and among all three factors ($F_{[7,256]} = 5.277$; $p < 0.001$). Post hoc analysis revealed that, on day 14 and day 16, AD(APP-E693Δ) neural cells were more vulnerable in the long culture than control neural cells and that DHA treatment rescued the vulnerability (*, $p < 0.001$).

(F) Typical images of Synapsin::EGFP neurons used in real-time survival assay. The scale bar represents 50 μm.

(G) Cytotoxicity in neural culture derived from control and AD iPSCs after treatment with DHA (5 μM) for 16 days. Measured fluorescent lactate dehydrogenase (LDH) release served as a measure of cytotoxicity. Data represent mean ± SD (n = 3 per clone). Two-way ANOVA showed significant main effects of DHA treatment ($F_{[1,32]} = 16.710$; $p < 0.001$) with a significant interaction between APP-E693Δ mutation and DHA treatment ($F_{[3,32]} = 9.210$; $p < 0.005$). There was a significant difference in AD(APP-E693Δ) neural cells between the DMSO-control and DHA groups (*, $p < 0.05$).

(H) Aβ40 and Aβ42 secreted from iPSC-derived neurons into medium (extracellular Aβ) at day 16 of the long-term culture were measured at 48 hr after the last medium change. Data represent mean ± SD (n = 3 per clone).

See also Figure S4 and Table S2.